

# Nonlinear tomographic reconstruction via nonsmooth optimization

Vasileios Charisopoulos<sup>\*1</sup> and Rebecca Willett<sup>†1,2,3</sup>

<sup>1</sup>Data Science Institute, University of Chicago

<sup>2</sup>Department of Computer Science, University of Chicago

<sup>3</sup>Computational and Applied Mathematics, Department of Statistics, University of Chicago

July 19, 2024

## Abstract

We study iterative signal reconstruction in computed tomography (CT), wherein measurements are produced by a linear transformation of the unknown signal followed by an exponential nonlinear map. Approaches based on pre-processing the data with a log transform and then solving the resulting linear inverse problem are tempting since they are amenable to convex optimization methods; however, such methods perform poorly when the underlying image has high dynamic range, as in X-ray imaging of tissue with embedded metal. We show that a suitably initialized subgradient method applied to a natural nonsmooth, nonconvex loss function produces iterates that converge to the unknown signal of interest at a geometric rate under the statistical model proposed by [Fridovich-Keil et al. \(2023\)](#). Our recovery program enjoys improved conditioning compared to the formulation proposed by the latter work, enabling faster iterative reconstruction from substantially fewer samples.

## 1 Introduction

A computed tomography (CT) scan is an imaging procedure in which a motorized X-ray source rotates rapidly around an object of interest, emitting narrow beams of X-rays at the object at varying angles. Detectors placed on the opposite side of the X-ray source measure the transmitted radiation, and the measurements are then combined to synthesize cross-sectional images of the object. In the context of medical imaging, for instance, the resulting images can be used for diagnostic purposes by clinicians; beyond the medical setting, CT imaging is also widely used in security settings ([TSA, 2024](#)), non-destructive material evaluation ([Center for Nondestructive Evaluation, Iowa State University, 2024](#)), archaeology ([Chhem and Brothwell, 2008](#)), and more. We refer the reader to [Buzug \(2011\)](#) for an overview of modern CT technologies.

Since the final images in CT scans are constructed from X-ray measurements at different angles, the number of collected measurements can heavily influence the quality of the final reconstruction. Indeed, reconstruction artifacts in medical CT scans can obstruct anatomical features that are important for therapy planning. However, large doses of radiation can have adverse effects on living tissue, highlighting the need for sample-efficient imaging techniques that use few measurements. At the same time, rapid reconstruction methods can increase the efficiency of radiology labs and reduce time-to-diagnosis.

Several commercial CT scanners rely on the following simple physical model ([Natterer, 2001](#)): let  $u \in \mathbb{R}^2$  denote a spatial index of the tissue being imaged, and suppose that the X-ray

---

<sup>\*</sup>[vchariso@uchicago.edu](mailto:vchariso@uchicago.edu)

<sup>†</sup>[willett@uchicago.edu](mailto:willett@uchicago.edu)

attenuation coefficient is given by a (unknown) function  $\mathcal{J} : \mathbb{R}^2 \rightarrow \mathbb{R}_+$ . If the initial beam intensity is  $I_0$ , the measured beam intensity across line  $\ell$ ,  $y_\ell$ , satisfies

$$y_\ell = I_0 \exp \left( - \int_\ell \mathcal{J}(u) du \right). \quad (1)$$

The goal of computed tomography is to recover the attenuation coefficients from measurements of the form (1). In practice, we have access to a limited number of measurements corresponding to a finite set of lines, indexed by a set of known angles  $\{\theta_1, \dots, \theta_m\}$ . In this case, we write

$$y_i = I_0 \exp(-\langle a_i, x_\star \rangle), \quad \text{for } i = 1, \dots, m, \quad (2)$$

where each  $a_i \in \mathbb{R}^d$ ,  $i = 1, \dots, m$  is a set of known coefficients derived from the Radon transform (Radon, 1917) at angle  $\theta_i$  and  $x_\star \in \mathbb{R}^d$  is a vector representation of the unknown image<sup>1</sup>; i.e., the  $j^{\text{th}}$  element of  $x_\star$  is  $\mathcal{J}(u_j)$ , where  $u_j$  is a discrete pixel location. To recover  $x_\star$ , commercial CT software applies a logarithmic preprocessing step to the  $y_i$  (Fu et al., 2017), resulting in a set of linear equations:

$$\langle a_i, x_\star \rangle = -\hat{y}_i, \quad i = 1, \dots, m, \quad \text{where} \quad \hat{y}_i = -\log \left( \frac{y_i}{I_0} \right). \quad (3)$$

The linear inverse problem in (3) is then solved using traditional methods, most commonly the so-called *filtered back-projection* (FBP) method. However, the logarithmic transform is numerically unstable as  $y_i \rightarrow 0$ , which is often the case for X-rays passing through high-density materials, and is known to lead to reconstruction artifacts (Gjesteby et al., 2016). To understand why this would impede recovery, consider the behavior of (3) as  $\|x_\star\|$  grows; the measurements  $y_i \rightarrow 0$  and the logarithmically transformed  $\hat{y}_i$  in (3) approaches  $-\infty$ . Therefore, the right-hand side of the linear system in (3) is sensitive to small perturbations in  $y_i$  (e.g., induced by numerical round-off errors). Since the Radon transform yields an ill-conditioned linear system, this means that we need many more samples to recover  $x_\star$  in a stable manner when the norm  $\|x_\star\|$  is larger. This motivates researchers and practitioners to consider iterative reconstruction methods that operate directly on (2).

Recently, Fridovich-Keil et al. (2023) studied iterative reconstruction from CT measurements under a Gaussian measurement model, intended to capture randomness in ray directions:

**Assumption 1** (Measurement model). The measurements satisfy<sup>2</sup>

$$y_i = 1 - \exp(-\langle a_i, x_\star \rangle_+), \quad i = 1, \dots, m, \quad \text{for} \quad [t]_+ := \max(t, 0), \quad (4)$$

where the sensing vectors are i.i.d. Gaussian:  $a_i \stackrel{\text{i.i.d.}}{\sim} \mathcal{N}(0, I_d)$ , for  $i = 1, \dots, m$ .

Given Assumption 1, they propose to recover  $x_\star$  by optimizing the following nonlinear least-squares objective using gradient descent:

$$\hat{x} = \underset{x \in \mathbb{R}^d}{\operatorname{argmin}} \frac{1}{2m} \sum_{i=1}^m (y_i - (1 - \exp(-\langle a_i, x \rangle_+)))^2, \quad (5)$$

While working with the measurements directly avoids numerical instability, the optimization problem in (5) is nonconvex; consequently, iterative methods like gradient descent are not guaranteed to converge to the solution  $x_\star$ . Moreover, it is possible that the conditioning of the problem in (5) is such that iterative methods are rendered impractical due to slow convergence. Nevertheless, Fridovich-Keil et al. (2023) argue that (5) can be solved to global optimality and provide a rigorous proof for their claim under the Gaussian measurement model. Their main findings are summarized below:

<sup>1</sup>While the unknown signal is typically 2D or 3D, we work with the vectorized representation for simplicity.

<sup>2</sup>Since  $\langle a_i, x_\star \rangle$  represents the line integral in the original model (2) and is nonnegative by construction, the proposed model in (4) enforces nonnegativity by taking the positive part of the inner product.

**Theorem 1.1** (Informal; adapted from (Fridovich-Keil et al., 2023, Theorem 1)). *Let Assumption 1 hold and suppose that the number of measurements  $m$  satisfies  $m \gtrsim \frac{e^{c\|x_\star\|}}{\|x_\star\|^2} \cdot d$ . Then solving (5) using gradient descent with stepsize  $\eta$  and careful initialization produces a sequence of iterates  $\{x_k\}_{k \geq 1}$  satisfying*

$$\|x_k - x_\star\|^2 \leq (1 - \eta e^{-5\|x_\star\|})^k \|x_\star\|^2, \quad (6)$$

*as long as  $\eta \lesssim e^{-5\|x_\star\|}$ , with high probability over the choice of design vectors.*

The result of Theorem 1.1 is positive and surprising: it suggests that, despite nonconvexity, the optimization problem in (5) can be solved reliably and efficiently with a simple first-order method initialized in a rather simple way: namely, by taking a “long” gradient descent step at  $x_0 = \mathbf{0}$  (see Theorem 1 in Fridovich-Keil et al. (2023) for a precise statement). However, some important limitations can be gleaned from Theorem 1.1:

**(Sample complexity)** The number of samples,  $m$ , scales exponentially with the norm of the unknown signal  $x_\star$ , and this norm can be large in settings of interest. This requirement is at odds with our desire to minimize exposure to radiation in practical settings.

**(Conditioning)** The “condition number”  $\exp(5\|x_\star\|)$  of the optimization problem — which is a natural measure of difficulty governing the speed of convergence of iterative methods — also scales exponentially with the norm of  $x_\star$ . As a result, convergence is not guaranteed unless the algorithm uses vanishingly small stepsizes. Consequently, the number of iterations (and computation time) required for reconstruction can be rather large.

A natural question is whether these limitations are essential or can be sidestepped by choosing a different objective function or reconstruction method. In this paper, we show that using a nonsmooth loss function — namely, the least absolute deviation ( $\ell_1$ ) penalty — yields **exponential improvements in both sample complexity and problem conditioning**. Our main finding is the following:

*Under the Gaussian measurement model,  $x_\star$  can be recovered from a **polynomial** number of measurements by solving a nonsmooth ( $\ell_1$ ) recovery program, whose conditioning is also **polynomial** in  $\|x_\star\|$ .*

Solving the aforementioned recovery program can be accomplished with standard first-order methods; the main method analyzed in our paper is the subgradient method using a scaled Polyak step-size (Polyak, 1969). A quantitative comparison between the guarantees of Fridovich-Keil et al. (2023) and ours can be found in Table 1; there, “iteration complexity” indicates the number of iterations needed for the estimation error to fall below a target level  $\varepsilon$  and “sample complexity” indicates the minimum number of samples  $m$  needed for the iteration complexity bounds to be valid.

In the next section, we formalize the measurement model and loss function used and provide a high-level overview of the proposed method and the key points of its convergence analysis.

## 1.1 Method overview

In this section, we provide a high-level overview of our method. Working under Assumption 1, we propose optimizing the following nonsmooth ( $\ell_1$ ) penalty:

$$f(x) := \frac{1}{m} \sum_{i=1}^m |y_i - h_i(x)|, \quad h_i(x) := 1 - \exp(-\langle a_i, x \rangle_+). \quad (7)$$

Method	Iteration complexity	Sample complexity
PolyakSGM (Alg. 1)	$O\left(\ x_\star\ ^6 \log\left(\frac{\ x_\star\ }{\varepsilon}\right)\right)$	$O(\ x_\star\ ^4 \cdot d)$
AdPolyakSGM (Alg. 2)		
GD (Fridovich-Keil et al., 2023)	$O\left(\exp(c_1 \ x_\star\ ) \log\left(\frac{\ x_\star\ }{\varepsilon}\right)\right)$	$O\left(\frac{\exp(c_2 \ x_\star\ )}{\ x_\star\ ^2} \cdot d\right)$

**Table 1:** Iteration and sample complexity of iterative reconstruction methods. The proposed methods achieve exponential gains in both metrics. For a formal statement of our results, see Theorem 3.1 (Algorithm 1) and Proposition 3.1 (Algorithm 2).

---

**Algorithm 1** PolyakSGM: Subgradient method with scaled Polyak stepsize

---

- 1: **Input:**  $x_0 \in \mathbb{R}^d$ , scaling  $\eta \in (0, 1]$ , budget  $K \in \mathbb{N}$ , optimal value  $f_\star$ .
  - 2: **for**  $k = 1, 2, \dots, K$  **do**
  - 3:   Set  $x_{k+1} := x_k - \eta \cdot \frac{f(x_k) - f_\star}{\|v_k\|^2} v_k$ , where  $v_k \in \partial f(x_k)$ .
  - 4: **return**  $x_K$ .
- 

To optimize  $f(x)$  in (7), we will use the subgradient method with Polyak stepsize, starting at  $x_0 = \mathbf{0}$  (see Algorithm 1 for a formal description of the method). Note that the optimal value  $f_\star = f(x_\star) = 0$  when the measurements are not corrupted by noise.

In Algorithm 1,  $\partial f(x)$  denotes the so-called *Clarke* subdifferential (Clarke, 1975), an appropriate generalization of the convex subdifferential for arbitrary Lipschitz functions. Like its convex counterpart, the Clarke subdifferential is set-valued mapping in general. The Clarke subdifferential of the loss function in (7) can be calculated with the help of the chain rule:

$$\partial f(x) = \frac{1}{m} \sum_{i=1}^m \mathbf{sign}(y_i - h_i(x)) \cdot (-e^{-\langle a_i, x \rangle_+}) a_i \mathbb{1}\{\langle a_i, x \rangle \geq 0\}, \quad (8a)$$

$$\text{where } \mathbf{sign}(x) := \begin{cases} 1, & x > 0, \\ -1, & x < 0, \\ [-1, 1], & x = 0, \end{cases} \quad \text{and} \quad \mathbb{1}\{x \geq 0\} := \begin{cases} 1, & x > 0 \\ 0, & x < 0, \\ [0, 1] & x = 0. \end{cases} \quad (8b)$$

**Remark 1.** Our implementation uses  $\mathbf{sign}(0) = 0$  and  $\mathbb{1}\{x \geq 0\} = 1$  if  $x = 0$  in (8b).

Much of our analysis will focus on showing that the loss  $f$  in (7) is “well-conditioned” in a neighborhood of the solution  $x_\star$ , a consequence of the following two regularity properties:

**(Lipschitz continuity)** There is  $L > 0$  such that for any  $x, \bar{x} \in \mathbb{R}^d$ , the loss  $f$  satisfies

$$|f(x) - f(\bar{x})| \leq L \|x - \bar{x}\|. \quad (9)$$

**(Sharp growth)** There is  $\mu > 0$  such that for any  $x$  near  $x_\star$ , the loss  $f$  satisfies

$$f(x) - f(x_\star) \geq \mu \|x - x_\star\|. \quad (10)$$

It is well known (see, e.g., Polyak (1969); Goffin (1977)) that classical subgradient methods converge linearly for *convex* functions satisfying (9)–(10), with rate

$$\|x_k - x_\star\|^2 \leq \left(1 - \frac{1}{\kappa^2}\right)^k \|x_0 - x_\star\|^2, \quad \kappa := \frac{L}{\mu}. \quad (11)$$

In (11), the **condition number**  $\kappa$  generalizes the classical notion of conditioning from smooth optimization to nonsmooth programs. Unfortunately, the loss in (7) is nonconvex; however, we show that it satisfies a key “aiming” condition, postulating that subgradients — potential search directions for Algorithm 1 — point to the direction of the solution  $x_\star$ .

$$(\text{Aiming}) : \min_{v \in \partial f(x)} \langle v, x - x_\star \rangle \geq \mu \|x - x_\star\|, \text{ for all } x \in \mathcal{B}(\mathbf{0}; 3\|x_\star\|) \setminus \{0\}. \quad (12)$$

The aiming inequality (12) serves two purposes: first, it is a key stepping stone to establishing the sharp growth property (10) in a neighborhood of  $x_\star$ . Moreover, it ensures that Algorithm 1 (with sufficiently small scaling  $\eta$ ) decreases the distance to  $x_\star$  monotonically:

$$\|x_{k+1} - x_\star\|^2 \leq \|x_k - x_\star\|^2 - \frac{\eta \mu f(x_k)}{\|v_k\|^2} \|x_k - x_\star\| < \|x_k - x_\star\|^2.$$

The focal point of our analysis is establishing (12) and showing that the moduli of sharp growth and Lipschitz continuity,  $\mu$  and  $L$ , do not scale with the dimension  $d$ . Indeed, we prove that

$$\mu = \Omega\left(\frac{1}{\|x_\star\|^2}\right) \text{ and } L = O(1), \text{ as long as } m = \Omega(d\|x_\star\|^4), \quad (13)$$

with high probability when the measurement vectors  $a_i$  are drawn from a standard Gaussian distribution; a precise statement can be found in Theorem 3.1. This establishes that the condition number of our problem satisfies

$$\kappa = O(\|x_\star\|^2),$$

i.e., it grows polynomially with the norm of the solution  $x_\star$ . As discussed previously (and illustrated in Table 1), this yields an exponential improvement over the sample and iteration complexity of the method in (Fridovich-Keil et al., 2023), which minimizes a smooth penalty using gradient descent. Though at first surprising, the advantage of nonsmooth formulations in signal recovery problems is well-documented in prior work (Li et al., 2020; Charisopoulos et al., 2021) showing that the  $\ell_1$  penalty is both better-conditioned and more robust to measurement noise than the squared  $\ell_2$  loss. Finally, we note that our convergence result can be extended to structured signal recovery by incorporating appropriate convex constraints as in Fridovich-Keil et al. (2023, Theorem 2). Since the proof techniques are similar, we do not pursue this generalization in our paper.

**Paper outline.** In the remainder of this section, we discuss related work (Section 1.2) and review standard notation and constructions from nonsmooth analysis and high-dimensional probability used throughout the paper (Section 1.3). In Section 2, we prove that the loss function (7) satisfies certain regularity properties, treating the initialization separately in Section 2.1. In Section 3 we analyze the convergence of Algorithm 1 and propose a variant that adapts to the unknown parameter  $\|x_\star\|$  in Section 3.1. Section 4 presents a set of numerical experiments that demonstrate the behavior of our method and its competitiveness with the approach of (Fridovich-Keil et al., 2023). We conclude with a discussion of the limitations of our approach and potential extensions of our work in Section 5. Proofs of all technical results are deferred to Appendix A.

## 1.2 Related work

Several algorithms for CT image reconstruction, including the standard FBP method, can be viewed as discrete approximations of analytical inversion formulas and are relatively inexpensive to implement, in contrast to iterative reconstruction (IR) methods. While there are reasons beyond computational complexity impeding the integration of iterative methods in CT hardware, as discussed in the survey of Pan et al. (2009), advances in computing and algorithm

designed have led to renewed interest in such methods (Beister et al., 2012; Geyer et al., 2015). While a comprehensive overview of IR methods is beyond the scope of this article, and can be found in surveys such as (Beister et al., 2012; Willemink et al., 2013), several of these methods are motivated by advances in numerical optimization: examples include the classical algebraic reconstruction technique (ART) (Gordon, 1974), which employs the Kaczmarz algorithm for iteratively solving linear systems (Kaczmarz, 1993); the SAGE method of Fessler and Hero (1994), which uses alternating minimization to accelerate the expectation-maximization (EM) method; the ASD-POCS method of Sidky and Pan (2008), inspired by total-variation (TV) regularization for image recovery (Rudin et al., 1992); and the nonconvex ADMM approach of Barber and Sidky (2024). Few of these works provide estimates on the sample and computational efficiency of the proposed methods and, when they do, the estimates are typically not adapted to CT problems. Finally, note that commercial iterative methods for CT imaging also incorporate proprietary knowledge, such as machine geometry and detector characteristics, to improve algorithm design (Willemink et al., 2013).

Beyond computed tomography, several works design and analyze first-order methods for signal recovery in other settings; this includes works that study the sample and computational complexity of recovering a signal from magnitude-only or quadratic measurements (Soltanolkotabi, 2019) (also known as *phase retrieval*) and measurements produced by piecewise nonlinearities such as ReLUs (Soltanolkotabi, 2017; Frei et al., 2020), as well as recovering low-rank matrices using the Burer-Monteiro factorization (Ma et al., 2020; Charisopoulos et al., 2021). Other works include (Mei et al., 2018), who develop a framework for transferring guarantees from population to empirical risk for smooth loss functions and (Chandrasekher et al., 2023), which develops nonasymptotic predictions for the trajectory of certain first-order methods using Gaussian data. To the best of our knowledge, the work of Fridovich-Keil et al. (2023) is the first to study the computational and sample complexity of signal recovery under the particular measurement model used in computed tomography.

### 1.3 Notation and basic constructions

We write  $\langle X, Y \rangle := \text{Tr}(X^\top Y)$  for the Euclidean inner product and  $\|X\| = \sqrt{\langle X, X \rangle}$  for the induced norm. We denote the unit sphere in  $d$  dimensions by  $\mathbb{S}^{d-1}$  and the Euclidean ball centered at  $\bar{x}$  and radius  $r$  by  $\mathcal{B}(\bar{x}; r)$ . When  $A \in \mathbb{R}^{m \times d}$ , we will write  $\|A\|_F = \sqrt{\langle A, A \rangle}$  for its *Frobenius* norm and  $\|A\|_{\text{op}} := \sup_{x \in \mathbb{S}^{d-1}} \|Ax\|$  for its *spectral* norm. Some of our guarantees depend on the complementary Gaussian error function,  $\text{erfc}(t)$ , defined by

$$\text{erfc}(t) = \frac{2}{\sqrt{\pi}} \int_t^\infty \exp(-u^2) du. \quad (14)$$

Finally, we will write  $A \lesssim B$  to indicate that there exists a constant  $c > 0$  such that  $A \leq cB$ ; the precise value of  $c$  may change from occurrence to occurrence.

**Orlicz norms.** We write  $\|X\|_{\psi_q}$  for the  $q$ -Orlicz norm (Orlicz, 1932) of a random variable  $X$ :

$$\|X\|_{\psi_q} := \inf \left\{ t > 0 \mid \mathbb{E} \left[ \exp \left( \left( \frac{|X|}{t} \right)^q \right) \right] \leq 2 \right\} \in [0, \infty].$$

Any  $X$  with  $\|X\|_{\psi_1} < \infty$  is called *subexponential*; any  $X$  with  $\|X\|_{\psi_2} < \infty$  is called *subgaussian*.

**Nonsmooth analysis.** Consider a locally Lipschitz function  $f : \mathbb{R}^d \rightarrow \mathbb{R}$  and a point  $x$ . The *Clarke subdifferential* of  $f$  at  $x$  (Clarke, 1975), denoted by  $\partial f(x)$ , is the convex hull of limits of gradients evaluated at nearby points:

$$\partial f(x) := \text{conv} \left\{ \lim_{i \rightarrow \infty} \nabla f(x_i) \mid x_i \xrightarrow{\Omega} x \right\}, \quad (\text{Clarke})$$

where  $\Omega \subset \mathbb{R}^d$  is the set of points at which  $f$  is differentiable. In particular, if  $f$  is  $L$ -Lipschitz on an open set  $U$ , then all  $x \in U$  and  $v \in \partial f(x)$  satisfy  $\|v\| \leq L$  (and vice-versa).

## 2 Regularity properties of the loss function

In this section, we show that the loss function satisfies certain regularity properties, including Lipschitz continuity (Section 2.2) and sharp growth (Section 2.3). We address the initial point  $x_0 = \mathbf{0}$  separately, establishing that the first iterate  $x_1$  is positively correlated with  $x_\star$  and bounded away from 0 to facilitate the use of the analytical framework outlined in Section 1.1.

### 2.1 Properties at initialization

We show that when  $x_0 = \mathbf{0}$ , the first iterate attains nontrivial correlation with the solution  $x_\star$ . To do so, we analyze the different components making up the first subgradient step.

**Lemma 2.1.** *The loss function satisfies*

$$\mathbb{P} \left( \left| f(0) - \frac{1}{2} \left( 1 - \exp \left( -\frac{\|x_\star\|^2}{2} \right) \operatorname{erfc} \left( \frac{\|x_\star\|}{\sqrt{2}} \right) \right) \right| \geq \|x_\star\| \sqrt{\frac{d}{m}} \right) \leq 2 \exp(-d). \quad (15)$$

An immediate consequence of Lemma 2.1 is that  $f(0)$  is of size  $\Omega(1)$  when  $\|x_\star\| = \Omega(1)$ .

**Corollary 2.1.** *For any  $x_\star$  such that  $\|x_\star\| \geq 1$  and  $m \gtrsim d \cdot \|x_\star\|^2$ , it holds that*

$$\mathbb{P} \left( f(0) \leq \frac{1}{5} \right) \leq \exp \left( -\frac{d}{2} \right), \quad (16)$$

where  $c > 0$  is a universal constant.

The next Lemma shows that a subgradient at 0 is bounded and correlated with  $-x_\star$ , leading to sufficient decrease in distance in the first step of Algorithm 1.

**Lemma 2.2.** *Consider the following subgradient at 0:*

$$v_0 := -\frac{1}{m} \sum_{i=1}^m a_i \mathbb{1} \{ \langle a_i, x_\star \rangle > 0 \} \in \partial f(0). \quad (17)$$

Then with probability at least  $1 - 2e^{-d}$ , it holds that

$$-\langle v_0, x_\star \rangle \geq \|x_\star\| \left( \sqrt{\frac{1}{2\pi}} - \sqrt{\frac{2d}{m}} \right), \quad (18a)$$

$$\|v_0\| \leq 1 + 2\sqrt{\frac{d}{m}}, \quad (18b)$$

$$\|x_1 - x_\star\| \leq \|x_\star\| \left( 1 - \frac{\eta}{10 \|x_\star\| \sqrt{\pi}} \right)^{1/2}, \quad (18c)$$

as long as  $m \gtrsim d$  and  $\eta \leq \frac{1}{2}$ .

### 2.2 Lipschitz continuity

We prove that the loss function is Lipschitz-continuous; note that the Lipschitz modulus is dimension-independent when  $m \gtrsim d$ .



**Proposition 2.1** (Lipschitz continuity). *The loss function is  $L$ -Lipschitz continuous, where  $L := 1 + 2\sqrt{\frac{d}{m}}$ , with probability at least  $1 - \exp(-d)$ :*

$$|f(x) - f(\bar{x})| \leq L \|x - \bar{x}\|, \quad \text{for all } x, \bar{x} \in \mathbb{R}^d. \quad (19)$$

This immediately implies the following upper bound on subgradient norms:

**Corollary 2.2.** *With probability at least  $1 - \exp(-d)$ , we have that*

$$\sup_{x \in \mathbb{R}^d} \max_{v \in \partial f(x)} \|v\| \leq 1 + 2\sqrt{\frac{d}{m}}. \quad (20)$$

## 2.3 Sharpness

In this section, we establish that the loss function  $f$  grows *sharply* away from its minimizer:

$$f(x) - f(x_\star) \geq \mu \|x - x_\star\|, \quad \text{for all } x \text{ “near” } x_\star,$$

where  $\mu = \frac{1}{4\sqrt{\pi}(1+9\pi\|x_\star\|^2)}$ . For technical reasons, we will prove this claim for all  $x \in \mathcal{B}(\mathbf{0}; 2\|x_\star\|)$ , as we will later show that all iterates of Algorithm 1 initialized at  $\mathbf{0}$  remain within that ball. Key to establishing the above claim is the following “aiming” inequality:

$$\min_{v \in \partial f(x)} \langle v, x - x_\star \rangle \geq \mu \|x - x_\star\|, \quad \text{for all } x \in \mathcal{B}(\mathbf{0}; 3\|x_\star\|) \setminus \{0\}. \quad (\text{Aiming})$$

The reason (Aiming) implies sharpness for  $f$  is captured in the following technical result:

**Lemma 2.3** (Solvability lemma). *Suppose  $f$  is Lipschitz on  $\mathcal{B}(\mathbf{0}; 3\|x_\star\|)$  and that the (Aiming) inequality holds. Then we have that*

$$f(x) - f_\star \geq \mu \min\{\|x - x_\star\|, \|x\|\}, \quad \text{for all } x \in \mathcal{B}(x_\star; \|x_\star\|). \quad (21)$$

**Remark 2.** While the lower bound furnished by Lemma 2.3 is weaker than the sharp growth inequality (10), our convergence analysis shows that the norm of the iterates produced by Algorithm 1 stays bounded away from 0 and, after an initial “burn-in” phase, surpasses the distance to  $x_\star$ . Consequently, (21) eventually reduces to the sharp growth property.

We now turn to the proof of the aiming inequality.

### 2.3.1 Proof of the aiming inequality

To establish (Aiming), we first derive a convenient expression for the inner product.

**Lemma 2.4** (Subdifferential inner product). *For any point  $x \in \mathbb{R}^d$ , we have that*

$$\begin{aligned} \langle \partial f(x), x - x_\star \rangle &= \frac{1}{m} \sum_{i=1}^m e^{-\langle a_i, x \rangle} |\langle a_i, x - x_\star \rangle| \mathbb{1}\{\langle a_i, x \rangle > 0\} \\ &\quad + \frac{1}{m} \sum_{i=1}^m \mathbb{1}\{\langle a_i, x \rangle = 0\} (\langle a_i, x_\star \rangle_+ + \mathbf{sign}(0) \langle a_i, x_\star \rangle_-). \end{aligned} \quad (22)$$

With the help of Lemma 2.4, we can establish the desired inequality in expectation.

**Lemma 2.5** (Aiming in expectation). *For any  $x \in \mathcal{B}(\mathbf{0}; 3\|x_\star\|) \setminus \{0\}$ , it follows that*

$$\mathbb{E}[\langle \partial f(x), x - x_\star \rangle] \geq \frac{\|x - x_\star\|}{\sqrt{8\pi}(1 + 9\pi\|x_\star\|^2)}. \quad (23)$$



Finally, we establish a uniform deviation inequality around the bound furnished by Lemma 2.5.

**Proposition 2.2.** *The following holds with probability at least  $1 - 2e^{-d}$ :*

$$\min_{x \in \mathcal{B}(\mathbf{0}; 3\|x_\star\|) \setminus \{x_\star, \mathbf{0}\}} \frac{\langle \partial f(x), x - x_\star \rangle}{\|x - x_\star\|} \geq \frac{1}{4\sqrt{\pi} (1 + 9\pi \|x_\star\|^2)}, \quad (24)$$

as long as  $m \gtrsim d \cdot \|x_\star\|^4$ .

### 3 Convergence analysis

In this section, we analyze the convergence of Algorithm 1. First, we denote

$$\bar{\rho} := \eta \left( \frac{\mu}{L} \right)^2 \frac{1}{40\sqrt{\pi} \|x_\star\|}, \quad \rho := \eta \left( \frac{\mu}{L} \right)^2, \quad \text{and} \quad T_0 := \left\lceil \frac{\log(2)}{\bar{\rho}} \right\rceil \quad (25)$$

for brevity. A quick discussion about their roles in the convergence analysis is in order:

- $\bar{\rho}$  is the contraction factor achieved while  $\|x_t - x_\star\| \geq \frac{1}{2} \|x_\star\|$ .
- $\rho > \bar{\rho}$  is the contraction factor achieved after  $\|x_t - x_\star\| < \frac{1}{2} \|x_\star\|$ .
- $T_0$  is an upper bound on the number of iterations elapsed until  $\|x_t - x_\star\| < \frac{1}{2} \|x_\star\|$ .

As the above quantities might suggest, our convergence analysis is split into two phases. Crucially, Algorithm 1 **does not** employ a different stepsize for the two phases: the distinction is only for theoretical purposes and – as demonstrated in Section 4 – does not affect the practical behavior of the method. For that reason, we believe it is just an artifact of our analysis.

We now turn to the analysis of the algorithm. We define the following events:

$$\mathcal{A}_{\text{slow}}(t) := \{ \|x_{t+1} - x_\star\|^2 \leq (1 - \bar{\rho}) \|x_t - x_\star\|^2 \}, \quad (26a)$$

$$\mathcal{A}_{\text{fast}}(t) := \{ \|x_{t+1} - x_\star\|^2 \leq (1 - \rho) \|x_t - x_\star\|^2 \}, \quad (26b)$$

$$\mathcal{B}_{\text{slow}}(t) := \left\{ \frac{1}{40\sqrt{\pi}} \leq \|x_t\| \leq 2 \|x_\star\| \right\}, \quad (26c)$$

$$\mathcal{B}_{\text{fast}}(t) := \left\{ \frac{1}{2} \|x_\star\| \leq \|x_t\| \leq 2 \|x_\star\| \right\}. \quad (26d)$$

We also recall that  $x_0 = \mathbf{0}$  and  $f_\star = 0$  throughout. Our analysis is inductive: initially, we note that Lemma 2.2 implies the following:

$$\|x_1 - x_\star\|^2 \leq \left( 1 - \frac{1}{20\sqrt{\pi} \|x_\star\|} \right) \|x_\star\|^2. \quad (27)$$

We now turn to a sequence of supporting Lemmas. The first one shows that the norms of the iterates remain bounded while the algorithm is in its “slow” phase.

**Lemma 3.1.** *We have that  $\{\mathcal{A}_{\text{slow}}(j)\}_{j \leq t} \implies \mathcal{B}_{\text{slow}}(t+1)$ .*

The next Lemma shows that the algorithm continues making progress (at a rate depending on  $\bar{\rho}$ ) while the iterates remain within the tube  $\mathcal{B}(\mathbf{0}; 2\|x_\star\|) \setminus \mathcal{B}(\mathbf{0}; 1/40\sqrt{\pi})$ .

**Lemma 3.2.** *We have that  $\{\mathcal{A}_{\text{slow}}(j)\}_{j < t}, \mathcal{B}_{\text{slow}}(t) \implies \mathcal{A}_{\text{slow}}(t)$  for any  $\eta \leq \frac{\mu}{L}$  and  $t \geq 1$ .*

The forthcoming Lemmas describe the behavior of the algorithm once iterates are in the ball  $\mathcal{B}(x_\star; \frac{1}{2}\|x_\star\|)$ . Lemma 3.3 shows that the algorithm indeed enters this region after sufficient progress; the remaining Lemmas mirror Lemmas 3.1 and 3.2.

**Lemma 3.3.** We have  $\{\mathcal{A}_{\text{slow}}(j)\}_{j < T_0} \implies \mathcal{B}_{\text{fast}}(T_0)$ .

**Lemma 3.4.** We have that  $\{\mathcal{A}_{\text{fast}}(j)_{T_0 \leq j < t}, \mathcal{B}_{\text{fast}}(t)\} \implies \mathcal{A}_{\text{fast}}(t)$  for any  $\eta \leq \frac{\mu}{L}$  and  $t \geq T_0$ .

**Lemma 3.5.** We have  $\{\mathcal{A}_{\text{fast}}(j)\}_{T_0 \leq j \leq t} \implies \mathcal{B}_{\text{fast}}(t+1)$ .

We are now ready to state our main convergence guarantee, which follows trivially from Lemmas 3.1 to 3.5. To that end, let

$$\kappa := 8\sqrt{\pi}(1 + 9\pi \|x_\star\|^2) \geq \frac{L}{\mu} \quad (28)$$

denote a bound on the condition number of the optimization problem. When  $\eta = \frac{\mu}{L}$ , we have

$$\rho = \eta \left(\frac{\mu}{L}\right)^2 \leq \kappa^{-3}, \quad \bar{\rho} = \rho \cdot \frac{1}{40\sqrt{\pi} \|x_\star\|} \geq \frac{1}{5} \rho \kappa^{-1/2}. \quad (29)$$

**Theorem 3.1** (Linear convergence of PolyakSGM). *Let Assumption 1 hold and suppose that the number of measurements  $m \gtrsim d \|x_\star\|^4$ , for  $\|x_\star\| \geq 1$ . Then Algorithm 1 with inputs  $x_0 = \mathbf{0}$ ,  $\eta \leq \frac{1}{\kappa}$ , where  $\kappa$  is defined in (28), and  $f_\star = 0$  produces a set of iterates  $\{x_i\}_{i=1,\dots}$  converging to  $x_\star$  at a linear rate:*

$$\|x_{i+1} - x_\star\|^2 \leq \begin{cases} (1 - \frac{1}{5}\eta\kappa^{-\frac{5}{2}}) \|x_i - x_\star\|^2, & i < T_0, \\ (1 - \eta\kappa^{-2}) \|x_i - x_\star\|^2, & i \geq T_0. \end{cases} \quad (30)$$

In particular, using the largest admissible stepsize  $\eta = \frac{1}{\kappa}$ , Algorithm 1 requires at most

$$\mathsf{T}(\varepsilon) \leq \left\lceil 7\kappa^{\frac{7}{2}} \right\rceil + \left\lceil 2\kappa^3 \log \left( \frac{\kappa}{\varepsilon} \right) \right\rceil \quad \text{subgradient evaluations}$$

to achieve estimation error  $\|x_t - x_\star\| \leq \varepsilon$ .

### 3.1 Adaptation to $\|x_\star\|$

In Theorem 3.1, the optimal  $\eta$  depends on the norm of the unknown signal  $x_\star$ , which affects the condition number  $\kappa$ . Here, we describe a data-driven approach to estimate that quantity at a constant expense. Recall the definition of  $\kappa$  in (28); the optimal  $\eta_\star$  in Theorem 3.1 is equal to  $\frac{1}{\kappa}$ . For any  $\hat{\kappa} \geq \kappa$  and  $\eta := \hat{\kappa}^{-1}$ , we have (during the second stage of the analysis):

$$\begin{aligned} \|x_t - x_\star\|^2 &\leq (1 - \eta\kappa^{-2})^t \|x_0 - x_\star\|^2 \\ &= (1 - \hat{\kappa}^{-1} \cdot \kappa^{-2})^t \|x_0 - x_\star\|^2 \\ &\leq (1 - \hat{\kappa}^{-3})^t \|x_0 - x_\star\|^2. \end{aligned} \quad (31)$$

In particular, a standard scheme to adapt  $\eta$  to the unknown  $\|x_\star\|$  (given a budget of  $T$  iterations) would proceed by setting  $\eta_i = \hat{\kappa}_i^{-1}$ , with  $\hat{\kappa}_1 = 1$ , and doubling  $\hat{\kappa}_{t+1} = 2\hat{\kappa}_t$  until the estimate (31) holds. To bypass the obvious issue – namely, that the distances  $\|x_j - x_\star\|$  are not available in practice – we use the following relationship (cf. Propositions 2.1 and 2.2):

$$\frac{1}{L} f(x_j) \leq \|x_j - x_\star\| \leq \frac{1}{\mu} f(x_j),$$

which leads to the following *computable* upper bound (valid for any  $\hat{\kappa} \geq \kappa$ ):

$$f(x_t) \leq \kappa \cdot (1 - \hat{\kappa}^{-3})^{t/2} f(x_0) \leq \hat{\kappa} (1 - \hat{\kappa}^{-3})^{t/2} f(x_0). \quad (32)$$

With (32) at hand, we describe our adaptation strategy below.

---

**Algorithm 2** AdPolyakSGM

---

**Input:**  $x_0 \in \mathbb{R}^d$ , target accuracy  $\varepsilon$ .

Set  $i = 0$ ,  $\widehat{\kappa}_i = 1$ .

**repeat**

$$T_i := \left\lceil 7\widehat{\kappa}_i^{\frac{7}{2}} \right\rceil + \lceil 2 \cdot \widehat{\kappa}_i^3 \log(\frac{\kappa_i}{\varepsilon}) \rceil$$

$$x_i := \text{PolyakSGM}(x_0, \widehat{\kappa}_i^{-1}, T_i, f_\star \equiv 0)$$

▷ Algorithm 1

$$\widehat{\kappa}_{i+1} = 2\widehat{\kappa}_i; i \leftarrow i + 1.$$

**until**  $f(x_i) \leq \varepsilon \cdot f(x_0)$

---

**Proposition 3.1.** *Let Assumption 1 hold and suppose that the number of measurements  $m \gtrsim d \|x_\star\|^4$ , for  $\|x_\star\| \geq 1$ . Then Algorithm 2 with  $x_0 = \mathbf{0}$  terminates after at most  $\log_2(\kappa)$  invocations of Algorithm 1 and returns a point  $\widehat{x}$  satisfying  $f(\widehat{x}) \leq \varepsilon f(x_0)$ . Moreover, it uses at most*

$$8\kappa^{\frac{7}{2}} + 3\kappa^3 \cdot \log\left(\frac{\kappa}{\varepsilon}\right) \quad \text{subgradient evaluations.}$$

**Remark 3.** Note that, since  $\kappa = \Theta(\|x_\star\|^2)$ , the cost of Algorithm 2 (as measured by the total number of subgradient evaluations) is just a constant factor worse compared to the cost of running Algorithm 1 with the optimal stepsize  $\eta_\star = \kappa^{-1}$ .

## 4 Numerical experiments

In this section, we evaluate our proposed algorithm in experiments using real and synthetic data. Our primary goal is to compare the performance of our method with the gradient-based algorithm introduced in (Fridovich-Keil et al., 2023); that work minimizes a squared version of the loss using gradient descent with constant stepsize:

$$\mathcal{L}(x) = \frac{1}{2m} \sum_{i=1}^m (1 - \exp(-\langle a_i, x \rangle_+) - y_i)^2, \quad (33a)$$

$$x_{k+1}^{\text{GD}} = x_k^{\text{GD}} - \eta_k \cdot \nabla \mathcal{L}(x_k^{\text{GD}}), \quad \eta_k = \begin{cases} c_0 \cdot e^{-5\|x_\star\|}, & k \geq 1, \\ \frac{4e^{-\frac{\|x_\star\|^2}{2}}}{\text{erfc}(\frac{\|x_\star\|}{\sqrt{2}})}, & k = 0, \end{cases} \quad (33b)$$

where  $c_0$  is a constant and  $x_0^{\text{GD}} = \mathbf{0}_d$  is used to initialize the method.

Our synthetic experiments use two different models for measurement vectors  $a_i$ :

**(Gaussian ensemble)** Every  $a_i$  satisfies  $a_i \sim \mathcal{N}(0, I_d)$ . This is the setting covered by our theoretical analysis (Theorem 3.1).

**(RWHT ensemble)** Every  $a_i$  is a row of a randomized Walsh-Hadamard transform with oversampling. Formally, given an oversampling factor  $\ell = \frac{m}{d} \in \mathbb{N}$ , we have

$$A = \begin{bmatrix} a_1^\top \\ a_2^\top \\ \vdots \\ a_m^\top \end{bmatrix} = \begin{bmatrix} H_d D_1 \\ H_d D_2 \\ \vdots \\ H_d D_\ell \end{bmatrix}, \quad \text{where } D_j = \text{diag}(\xi_1^{(j)}, \dots, \xi_d^{(j)}), \quad \xi_i^{(j)} \stackrel{\text{i.i.d.}}{\sim} \text{Unif}(\pm 1),$$

where  $H_d$  is the  $d \times d$  matrix implementing the Walsh-Hadamard transform. In order for  $H_d$  to be well-defined, we assume that  $d$  is an integer power of 2 for simplicity.

The operations  $v \mapsto Av$  and  $u \mapsto A^\top u$  can be implemented using  $O(d \log d)$  flops and  $O(m)$  memory using the Fast Walsh-Hadamard transform. This allows us to test our method for values of  $d$  that prohibit storing a dense  $m \times d$  matrix.

## 4.1 Comparison of PolyakSGM and gradient descent

### 4.1.1 Sample efficiency

We first study the sample efficiency of our method and gradient descent (33b). Recall that Theorem 1 in (Fridovich-Keil et al., 2023) provides convergence guarantees for the latter, requiring

$$m = \Omega\left(\frac{\exp(c\|x_\star\|)}{\|x_\star\|^2} \cdot d\right) \quad \text{samples,}$$

while our Theorem 3.1 only requires

$$m = \Omega(\|x_\star\|^4 \cdot d) \quad \text{samples,}$$

an exponential improvement. To check if this sample efficiency gap manifests in practice, we generate synthetic problem instances for varying signal scales  $\|x_\star\| \in \{1, 1.5, 2, \dots, 8\}$  and oversampling factors  $\frac{m}{d} \in \{2, 4, \dots, 16\}$ , using Gaussian measurements and a fixed dimension  $d = 128$ . We solve each instance with Algorithm 1 (with fixed  $\eta = 1$  across all instances) and gradient descent (with optimized step-size  $\eta$ , chosen to minimize the final estimation error, for each individual instance). We declare a solve successful if an estimate  $\hat{x}$  satisfying  $\|\hat{x} - x_\star\| \leq 10^{-5}$  is found within  $10^4$  iterations and calculate the empirical success probability over 25 independently generated problem instances for each configuration. The results of the experiment are depicted in Figure 1. We observe that gradient descent experiences a sharp cut-off in recovery probability, while Algorithm 1 can recover higher-energy signals with substantially fewer measurements.

### 4.1.2 Optimized stepsizes

We now compare the convergence behavior of Algorithm 1 against gradient descent (33b) on different synthetic problems. We use Algorithm 1 with pre-factor  $\eta = 1$ , corresponding to the stepsize originally proposed by Polyak (1969). To ensure a fair comparison, we experimented with different values of  $c_0$  for (33b), searching over a grid  $\{2^j \cdot \exp(5\|x_\star\|) \mid -3 \leq j \leq 3\}$  for each instance. We tried different values for the dimension  $d \in \{256, 512, 1024\}$  and oversampling ratios  $\frac{m}{d} \in \{4, 8\}$ . As the results in Figure 2 show, our method produces iterates that converge to the solution  $x_\star$  nearly an order of magnitude faster than the baseline method.

### 4.1.3 Theoretically prescribed stepsizes

Next, we compare Algorithm 1 equipped with the stepsize prescribed by Theorem 3.1:

$$\eta = \frac{1}{8\sqrt{\pi}(1 + 9\pi\|x_\star\|^2)}$$

against gradient descent with the stepsize proposed by (Fridovich-Keil et al., 2023), given in (33b). We posit that the primary advantage of our method stems from the milder dependence on  $\|x_\star\|$  and generate instances with  $\|x_\star\| \in \{1, 2, 4\}$  to verify this hypothesis. For our experiments, we fix the number of samples to  $m = d\|x_\star\|^4$ , as suggested by Theorem 3.1. The results in Figure 3 confirm that the convergence rate of our method decays more gracefully with the norm  $\|x_\star\|$ . At the same time, we observe that the gradient method stagnates when  $\|x_\star\| = 4$ , while our method does not; this may be due to the fact that  $m = d\|x_\star\|^4$  samples are below the sample complexity threshold from (Fridovich-Keil et al., 2023). Note that the initial iterate distance in Figure 3 appears lower for the gradient method due to the use of a carefully crafted initialization (33b).

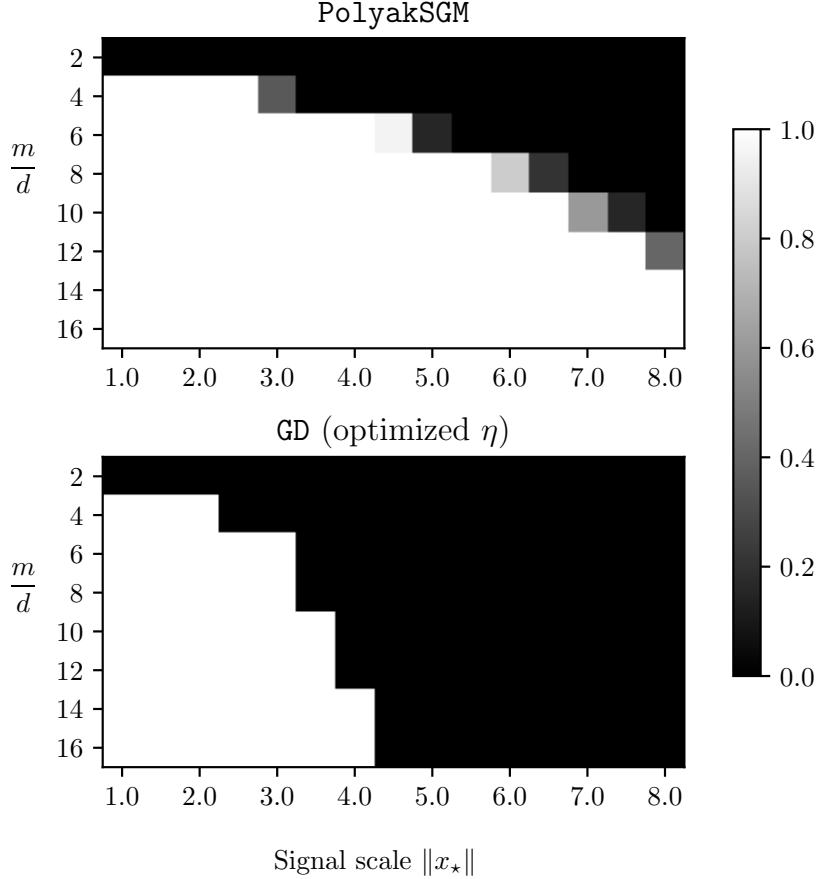


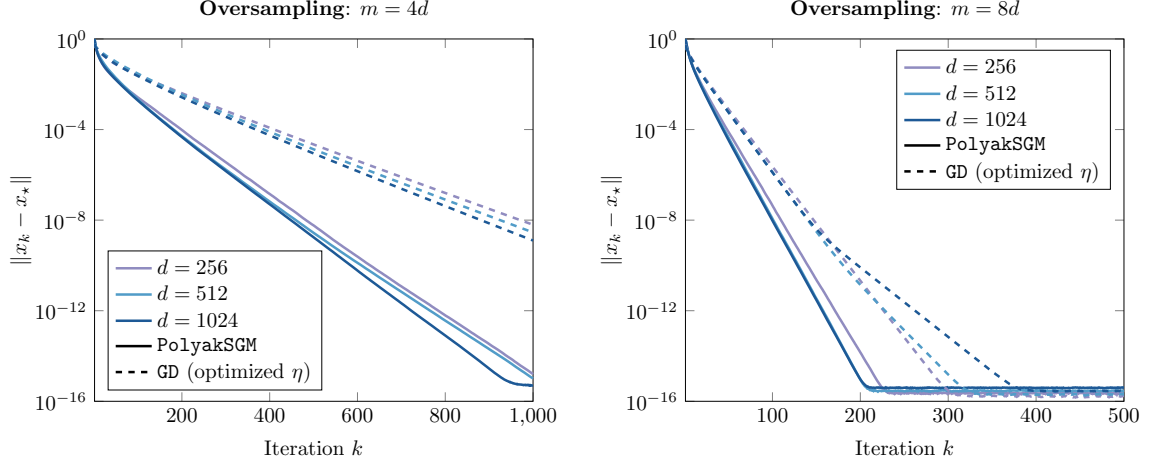
**Figure 1:** Empirical probability of recovering  $x_\star$  for various signal scales and oversampling factors over synthetic problems with  $d = 128$  and Gaussian measurements. The empirical probability for each configuration is calculated over 25 independently generated problem instances. Lighter tiles indicate higher probability of recovery. We compare Algorithm 1 with  $\eta = 1$  against gradient descent with optimized stepsize  $\eta$  using a logarithmically spaced grid.

#### 4.1.4 Robustness to stepsize misspecification

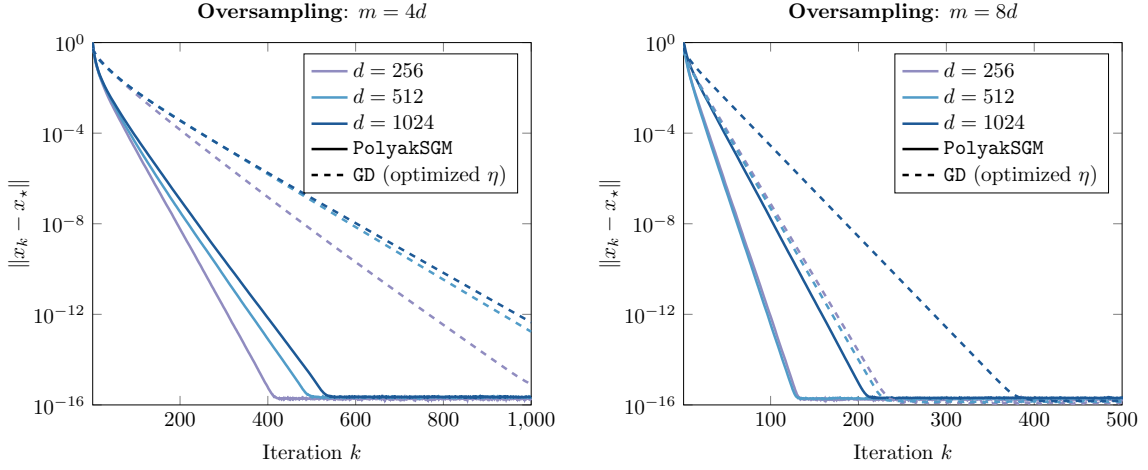
When deploying optimization methods, it is common to try a range of stepsizes and use the solution achieving the lowest loss. To that end, we conduct an experiment comparing the robustness of Algorithm 1 and (33b) to different stepsizes  $\eta$ . In particular, we report the number of iterations elapsed by each method to find a solution  $\hat{x}$  with distance  $\|\hat{x} - x_\star\| \leq \varepsilon$ , using  $\varepsilon = 10^{-5}$  and a maximal budget of  $10^4$  iterations (we terminate any run that has not achieved the target suboptimality within the iteration limit). We fix  $d = 256$ ,  $m = 4d$  and  $\|x_\star\| = 1$  and initialize both methods at  $x_0 = \mathbf{0}$ . We solve 10 independently generated instances for each configuration and report the median number of iterations  $\pm 3$  standard deviations; the results are shown in Figure 4. While the best configuration yields only slightly faster convergence for PolyakSGM compared to gradient descent, the latter method exhibits higher variance. We also observe that the discrepancy between best-performing and theoretically prescribed stepsizes is much starker for gradient descent compared to PolyakSGM, suggesting that the convergence analysis of gradient descent may be substantially improved.

## 4.2 Comparison of AdPolyakSGM and PolyakSGM

We compare the empirical performance of AdPolyakSGM (Algorithm 2) and PolyakSGM (Algorithm 1) on synthetic problems with measurements generated by Gaussian and RWHT ensem-



(a) Performance of Algorithm 1 against gradient descent with optimized stepsize  $\eta$  for measurement vectors  $a_i$ ,  $i = 1, \dots, m$  generated from a Gaussian ensemble.



(b) Performance of Algorithm 1 against gradient descent with optimized stepsize  $\eta$  for measurement vectors  $a_i$ ,  $i = 1, \dots, m$  generated from a randomized Walsh-Hadamard (RWHT) ensemble.

**Figure 2:** Comparison of PolyakSGM (Algorithm 1) using  $\eta = 1$  with gradient descent (33b) using tuned stepsize  $\eta$  for synthetic problems with Gaussian and randomized Walsh-Hadamard measurements. The iterates produced by Algorithm 1 converge to  $x_*$  at moderately faster rates.

bles. Recall that Proposition 3.1 implies that the iteration complexity of Algorithm 2 is at most a constant factor worse than that of the “optimal” version. Our experiments, shown in Figure 5, provide the following insights:

1. The standard Polyak stepsize (corresponding to  $\eta = 1$ ) already yields good performance.
2. The number of subgradient evaluations of Algorithm 2 is within a small constant factor of the “optimal” number, as predicted by our theory.

In particular, the first point above indicates that the standard Polyak step size might be sufficient to guarantee convergence for the CT problem. Although beyond the scope of this paper, a theoretical investigation of this phenomenon is an exciting direction for future work.

### 4.3 Effect of measurement noise

This section examines the performance of the proposed method in the presence of measurement noise. We start by discussing necessary algorithmic modifications: first, note that the presence

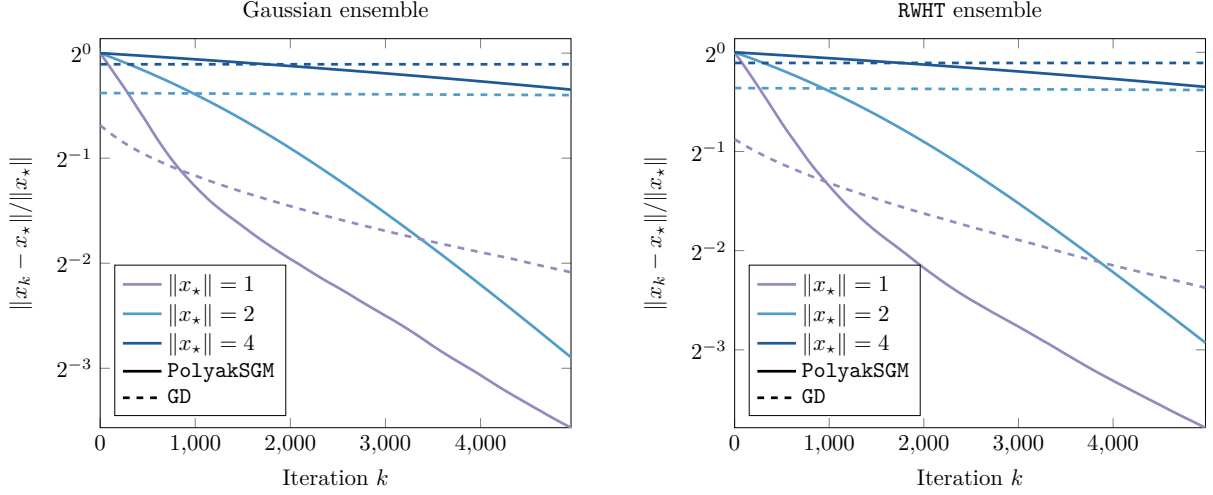


**Figure 3:** Comparison between Algorithm 1 and (33b) using theoretically prescribed stepsizes for synthetic problem instances. In all cases, Algorithm 1 converges faster than gradient descent.

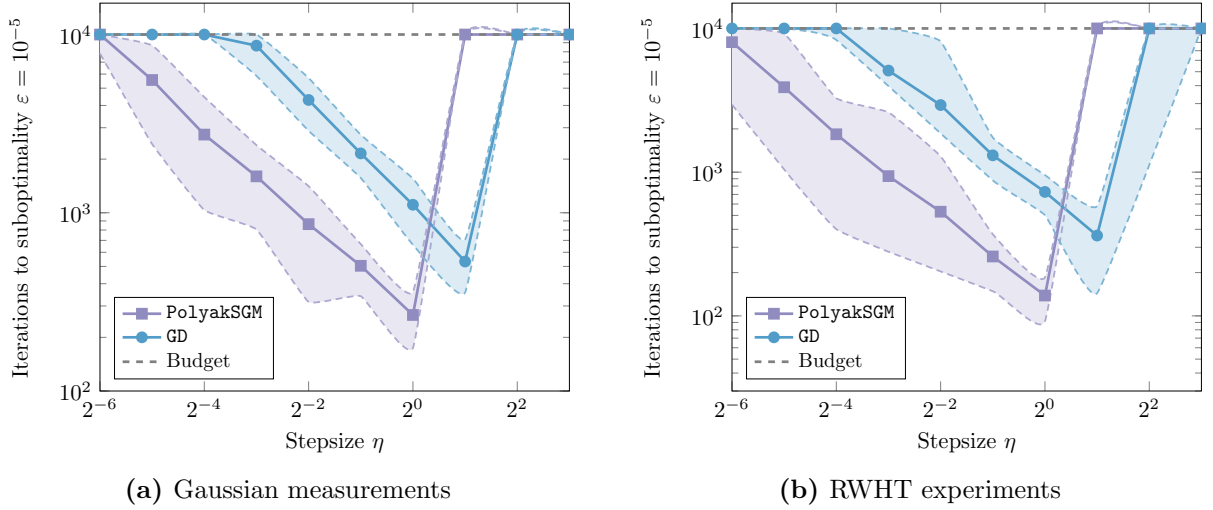


**Figure 4:** Number of iterations to achieve suboptimality of  $\varepsilon = 10^{-5}$  for Algorithm 1 and gradient descent for different stepsizes  $\eta$ . Reporting median over 10 independent runs (solid line)  $\pm 3$  standard deviations (shaded area); see Section 4.1.4 for description.

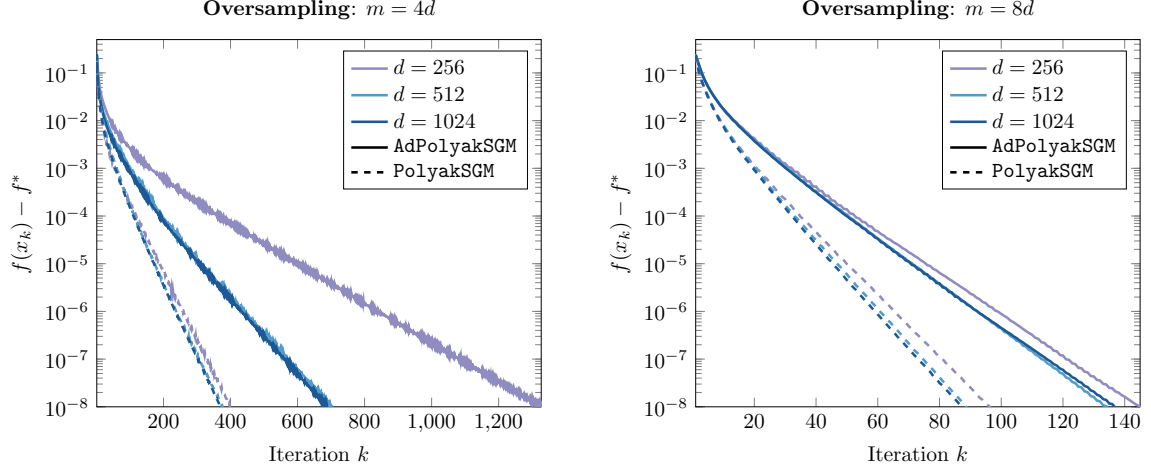
of noise implies that the optimal value of (7) is no longer  $f_\star = 0$ . While it is possible in theory to apply Algorithm 1 to problems with arbitrary optimal value  $f_\star$ , it is rarely the case that  $f_\star$  is known or easy to estimate a-priori. To remedy this, one can replace the Polyak step with a geometrically decaying stepsize, as suggested by Polyak (1969); Goffin (1977); Davis et al. (2018), or use the inner-outer loop structure proposed by Hazan and Kakade (2019) for problems where a lower bound  $\tilde{f} \leq f_\star$  is known. Since  $\tilde{f} = 0$  is always a valid lower bound in our setting, we opt for the latter approach; see Appendix D for a detailed description of Algorithm 3, which we use for these experiments.

Our experiments follow the Poisson noise model. This model is relevant for *photon-counting CT*, where instead of the energy of the beam incident to the detector at angle  $\theta_i$  we measure the raw number of particles reaching the detector. Herein, measurements satisfy

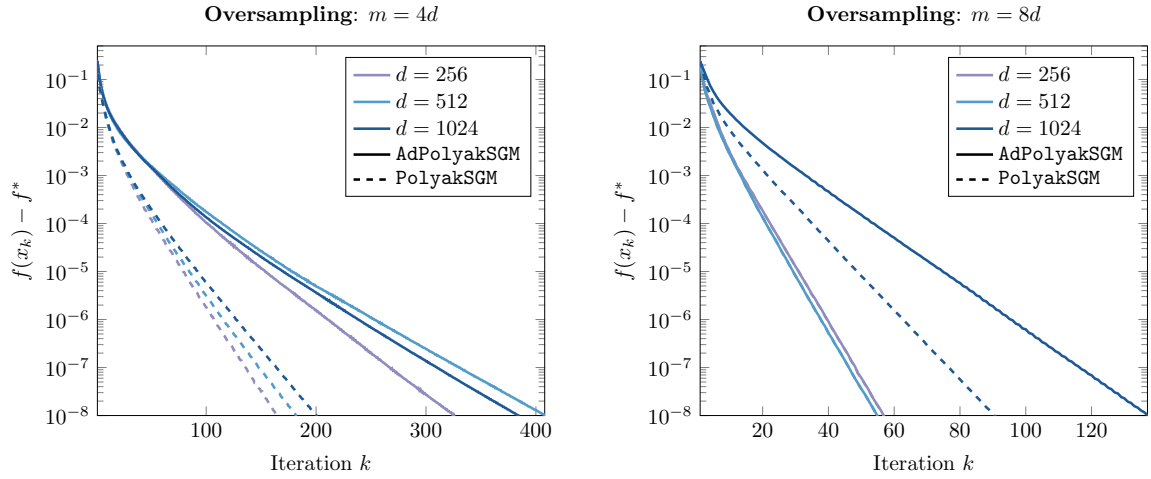
$$y_i \sim \text{Poisson}(S_i \cdot \exp(-\langle a_i, x_\star \rangle_+)), \quad i = 1, \dots, m,$$

where  $S_i > 0$  is determined by the sensitivity of the detector and the intensity of the X-ray





(a) Performance of Algorithm 1 with  $\eta = 1$  against Algorithm 2 for measurement vectors  $a_i$ ,  $i = 1, \dots, m$  generated from a Gaussian ensemble.



(b) Performance of Algorithm 1 with  $\eta = 1$  against Algorithm 2 for measurement vectors  $a_i$ ,  $i = 1, \dots, m$  generated from a randomized Walsh-Hadamard (RWHT) ensemble.

**Figure 5:** Comparison between Algorithm 1 and Algorithm 2 for synthetic problems with Gaussian and randomized Walsh-Hadamard measurements.

beam. For large  $S_i$ , we can use the following Gaussian approximation:

$$y_i \approx S_i \exp(-\langle a_i, x_\star \rangle_+) + \sqrt{S_i \exp(-\langle a_i, x_\star \rangle_+)} \cdot \xi_i, \quad \xi_i \sim \mathcal{N}(0, 1). \quad (34)$$

Our Poisson simulations use the model (34) and fix  $S_i \equiv S = 10^5$  for all detectors.

In what follows, we run a synthetic experiment with  $d = 128$  (Gaussian ensemble),  $d = 128 \times 128$  (RWHT ensemble), and  $m = 8 \cdot d$ , while varying the norm of the unknown signal  $\|x_\star\| \in \{2, 3, 4, 5\}$ . We then run Algorithm 3 with  $T_{\text{outer}} = 10$ ,  $T_{\text{inner}} = 1000$ ,  $x_0 = \mathbf{0}$  and  $\eta = 1$ , for a total budget of  $T_{\text{outer}} \times T_{\text{inner}} = 10^4$  subgradient evaluations, and compare against gradient descent with a budget of  $10^4$  iterations starting from the same initial point  $x_0$ . For each run of gradient descent, we optimize over a logarithmically-spaced grid  $\{2^j \mid j = -3, -2, \dots, 2, 3\}$  to pick the step-size  $\eta_k$ . The results of the experiment are shown in Figure 6, illustrating significant performance gains for Algorithm 3 compared to gradient descent across all configurations.

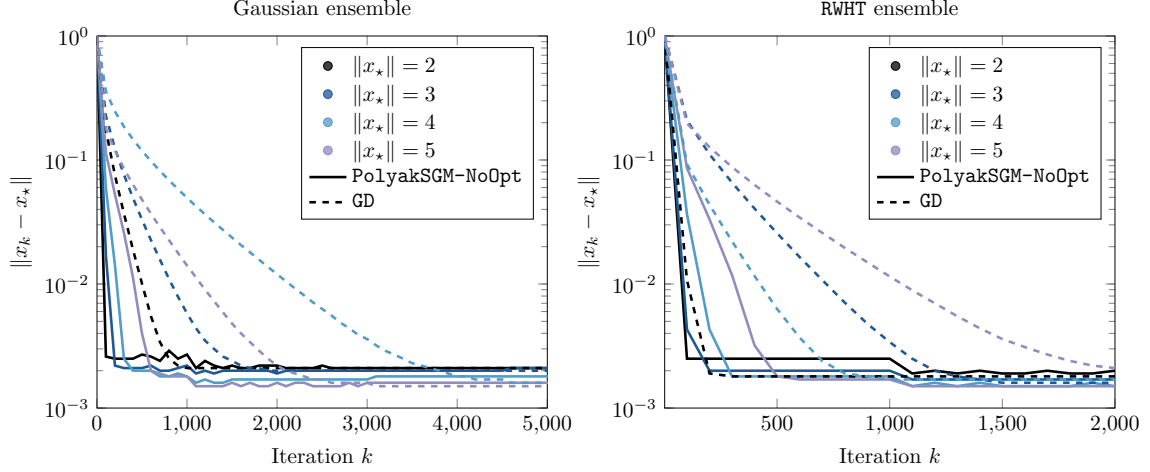


**Figure 6:** Convergence of Alg. 3 and gradient descent (GD) for problems with Poisson measurement noise (34). For a fixed budget of (sub)gradient evaluations, the two methods achieve similar estimation errors. However, Algorithm 3 typically converges to the minimal distance an order of magnitude faster than gradient descent.

#### 4.4 Experiments on CT imaging

We now turn to a more realistic model of X-ray CT imaging, wherein the unknown signal  $x_*$  is a vectorized version of an image  $I_* \in [0, 1]^{n \times n}$  and  $a_i$  is the  $i^{\text{th}}$  row of the discrete Radon transform applied to  $x_*$  at angle  $\theta_i$ . In a typical imaging setup, the number of measurements  $m \ll n^2$  and the resulting problem is ill-posed, necessitating the use of regularization in the form of constraints or penalties. In this section, we focus on total-variation (TV) regularization:<sup>3</sup>

$$\min_x \left\{ \frac{1}{m} \sum_{i=1}^m |y_i - h_i(x)| \mid \|\mathbf{M}(x)\|_{\text{TV}} \leq \lambda \right\}, \quad (35)$$

where  $\mathbf{M}(x) : \mathbb{R}^{n^2} \rightarrow \mathbb{R}^{n \times n}$  reshapes a vector to a square matrix of compatible shape and  $\|x\|_{\text{TV}}$  is the total variation norm proposed by (Rudin et al., 1992). Given  $x \in \mathbb{R}^{n^2}$  and  $X \in \mathbb{R}^{n \times n}$ ,

$$\mathbf{M}(x) = \begin{bmatrix} x_{1:n} & x_{(n+1):2n} & \cdots & x_{(n^2-n+1):n^2} \end{bmatrix}, \quad (36)$$

$$\|X\|_{\text{TV}} := \sum_{i,j} \sqrt{(X_{i+1,j} - X_{i,j})^2 + (X_{i,j+1} - X_{i,j})^2}. \quad (37)$$

To solve (35), we use the projected subgradient method; the steps of Algorithm 1 become

$$x_{k+1} := \text{proj}_{\mathcal{X}} \left( x_k - \eta \frac{f(x_k)}{\|v_k\|^2} v_k \right), \text{ where } v_k \in \partial f(x_k), \mathcal{X} := \{x \mid \|\mathbf{M}(x)\|_{\text{TV}} \leq \lambda\}. \quad (38)$$

The bottleneck in implementing (38) is the computation of the projection operator; we describe a simple iterative approach based on the Douglas-Rachford (DR) splitting method for computing the projection in Appendix C. For our experiments, we use the same iterative method to endow the gradient descent step in (33b) with a projection onto  $\mathcal{X}$ .

We now turn to our experiments, where we compare the reconstruction quality achieved by Algorithm 1 and gradient descent (33b) for recovering a  $128 \times 128$  Shepp-Logan phantom from CT measurements. We follow the experimental setup from Fridovich-Keil et al. (2023); namely, we enlarge the radius of one of the center ellipsoids of the Shepp-Logan phantom

<sup>3</sup>We focus on the constrained instead of the penalty version of TV regularization, since the Polyak stepsize cannot be used as-is in the presence of regularization penalties.

by a factor of 2 and adjust the corresponding pixel intensities in the range  $\{0.5, 1.0, 2.0\}$  to simulate the presence of different materials, and scale down all pixel intensity values by 4. We then run both methods from the same initialization  $x_0 = 0$  for 10000 iterations and visualize the reconstructions at  $k = 1000$ ,  $k = 5000$  and  $k = 10000$  iterations. We also report the peak signal-to-noise ratio (PSNR) achieved by each reconstruction method; given a ground truth image  $I_\star \in [0, 1]^{n_1 \times n_2}$  and a reconstruction  $\hat{I} \in [0, 1]^{n_1 \times n_2}$ , the PSNR of  $\hat{I}$  is

$$\text{PSNR}(\hat{I}; I) := -10 \log_{10} \left( \frac{1}{n_1 \cdot n_2} \left( \frac{\|\hat{I} - I\|_F}{\max_{i,j} |I_{ij}|} \right)^2 \right).$$

The reconstruction results are shown in Figure 7 for the center ellipsoid with low intensity and Figure 8 for the center ellipsoid with high intensity.<sup>4</sup> Qualitatively, the image found by gradient descent is much blurrier than that of Algorithm 1 and is unable to resolve the different ellipsoids in the earlier stages of reconstruction (Figures 7i, 7ii, 8i and 8ii). Additionally, the gradient descent reconstruction exhibits streak artifacts even for low pixel intensity values in the central ellipsoid, while Algorithm 1 only exhibits limited streak artifacts in the high-intensity setup. Quantitatively, the reconstruction PSNR achieved by Algorithm 1 is consistently much higher than that of gradient descent, with a 20% relative improvement at the final stage.

---

<sup>4</sup>To better illustrate the differences in reconstruction, we plot the square root of pixel intensity values.

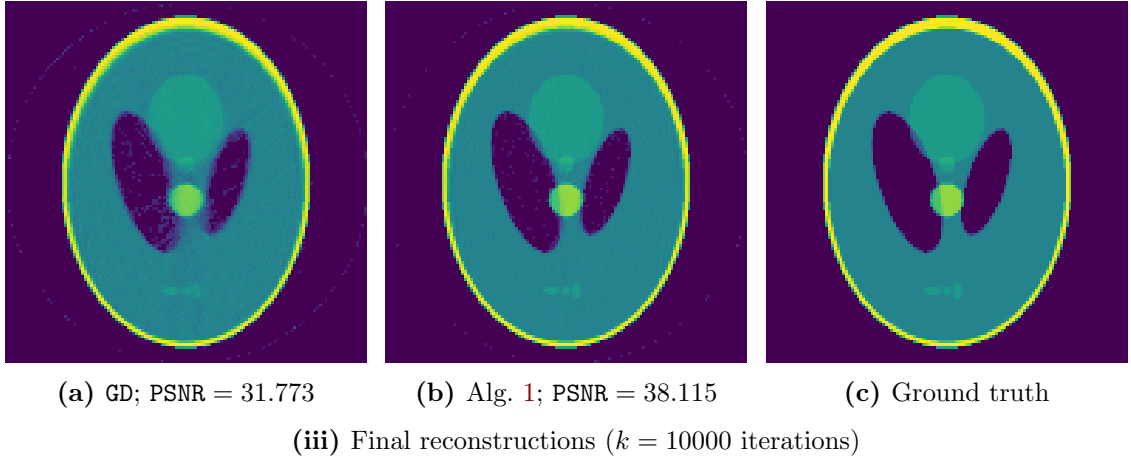
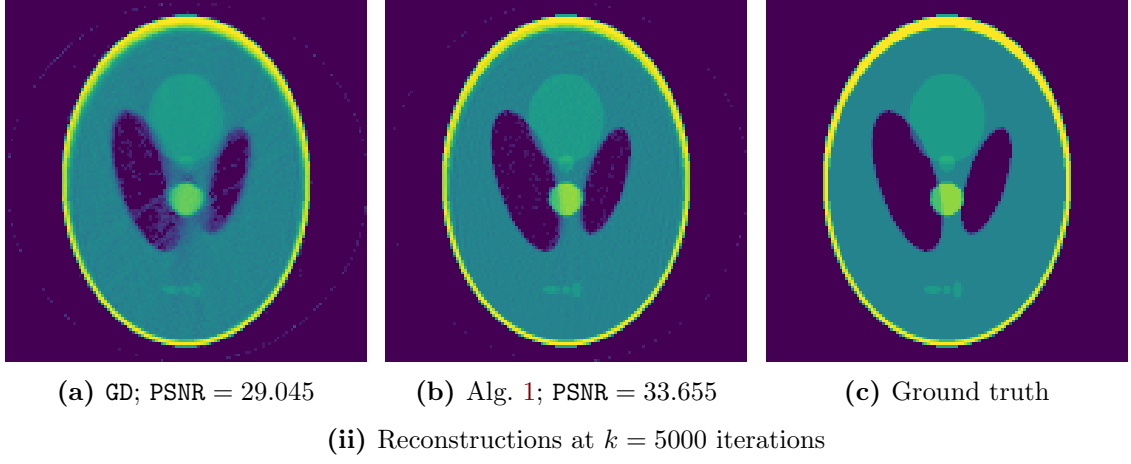
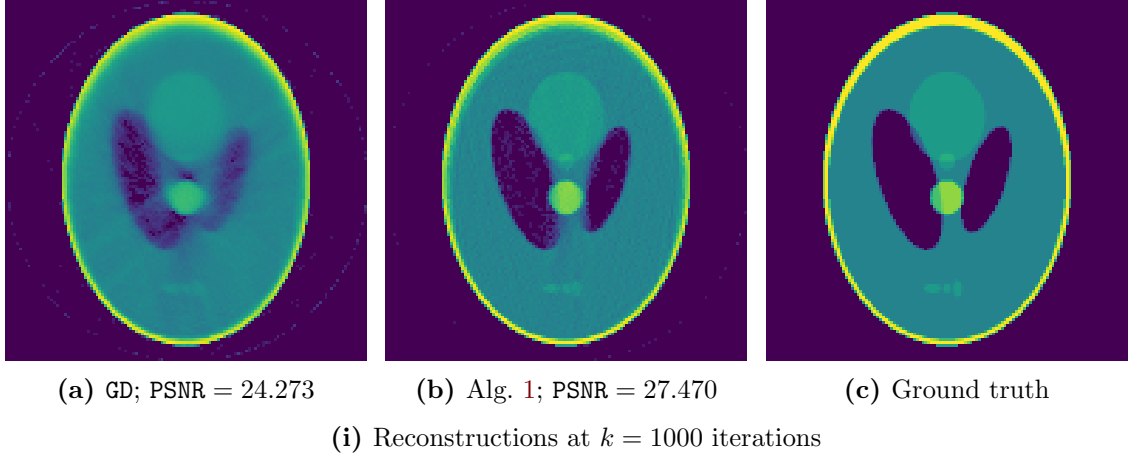
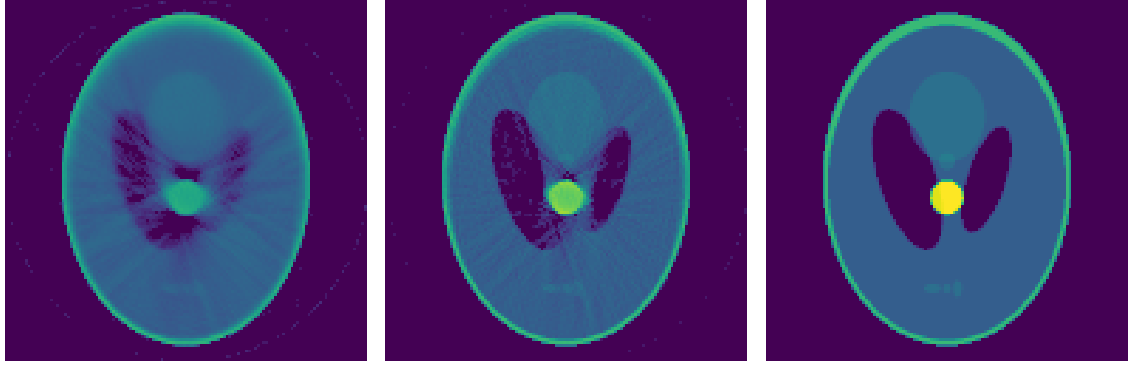


**Figure 7:** Comparison of reconstructions produced by gradient descent (33b), labeled GD, and Algorithm 1 for the modified Shepp-Logan phantom with low pixel intensity (0.5) in the center ellipsoid. Algorithm 1 is run with  $\eta = 1$ , while GD is run with  $\eta_0$  as specified in (33b) and  $\eta_k \equiv \eta_{\text{best}}$  for  $k \geq 1$ , where  $\eta_{\text{best}}$  is determined by optimizing over a logarithmically-spaced grid of values  $\{2^j \mid -3 \leq j \leq 3\}$ . Both algorithms were initialized at  $x_0 = 0$ .



(a) GD; PSNR = 24.998

(b) Alg. 1; PSNR = 29.055

(c) Ground truth

(i) Reconstructions at  $k = 1000$  iterations



(a) GD; PSNR = 28.652

(b) Alg. 1; PSNR = 34.906

(c) Ground truth

(ii) Reconstructions at  $k = 5000$  iterations



(a) GD; PSNR = 30.825

(b) Alg. 1; PSNR = 37.894

(c) Ground truth

(iii) Final reconstructions ( $k = 10000$  iterations)

**Figure 8:** Comparison of reconstructions produced by gradient descent (33b), labeled GD, and Algorithm 1 for the modified Shepp-Logan phantom with high pixel intensity (2.0) in the center ellipsoid. Algorithm 1 is run with  $\eta = 1$ , while GD is run with  $\eta_0$  as specified in (33b) and  $\eta_k \equiv \eta_{\text{best}}$  for  $k \geq 1$ , where  $\eta_{\text{best}}$  is determined by optimizing over a logarithmically-spaced grid of values  $\{2^j \mid -3 \leq j \leq 3\}$ . Both algorithms were initialized at  $x_0 = 0$ .

## 5 Discussion

There are several open questions and potential extensions to our work that we now discuss.

1. Our analysis assumes Gaussian observations, but design vectors corresponding to real CT measurements are typically sparse, nonnegative and highly structured; obtaining efficiency estimates in this setting is likely challenging. Nevertheless, it may be interesting to consider structured designs with limited randomness, such as random illumination angles.
2. Our theoretical results do not consider noisy measurements, such as those in the experiments of Section 4.3. The Poisson noise model, wherein the observed energy satisfies

$$y_i \sim \text{Poisson}(S \exp(-\langle a_i, x_\star \rangle_+)),$$

is of most relevance to photon-counting CT problems. We leave a theoretical investigation of the effects of different types of noise to future work.

3. Our current model does not take into account the polychromatic nature of the X-ray beam, which is typically distributed across a spectrum of energies (Elbakri and Fessler, 2003; Barber et al., 2016). This is an important modeling step, since attenuation coefficients of materials used in CT imaging typically vary across the energy spectrum. To address this, one could consider measurements of the form

$$y_i = \sum_{j=1}^{n_E} S_j \exp(-\zeta_j \langle a_i, x_\star \rangle_+), \quad i = 1, \dots, m,$$

where  $S_j$  is the intensity of the beam at energy level  $j$ ,  $n_E$  is the number of distinct energy levels considered – resulting from a discretization of the energy spectrum – and  $\zeta_j$  models a different known attenuation coefficient per energy level.

4. Empirically, we observe that the Polyak stepsize without any modification (i.e., Algorithm 1 with  $\eta = 1$ ) performs best across all instances. A potential explanation is that the optimization problem (7) possesses “benign landscape” around  $x_0 = \mathbf{0}$ , so that a few Polyak steps guide iterates towards a local basin of attraction, wherein the conditioning of the loss function is much better than our estimate. While it is unrealistic to expect the condition number to be independent of  $\|x_\star\|$ , obtaining the “optimal” dependence is an interesting direction for future work.
5. Finally, another potential direction for future research is expanding the algorithmic toolkit applied to the problem (7). For example, it may be desirable to solve (7) with stochastic methods and/or using better local models for the objective function (Asi and Duchi, 2019; Davis et al., 2023).

## Acknowledgements

We thank Damek Davis and Emil Sidky for helpful discussions. VC and RW gratefully acknowledge the support of AFOSR FA9550-18-1-0166, NSF DMS-2023109, DOE DE-SC0022232 and the Margot and Tom Pritzker Foundation.

## References

- Asi, H. and Duchi, J. C. (2019). Stochastic (approximate) proximal point methods: Convergence, optimality, and adaptivity. *SIAM Journal on Optimization*, 29(3):2257–2290.
- Barber, R. F. and Sidky, E. Y. (2024). Convergence for nonconvex ADMM, with applications to CT imaging. *Journal of Machine Learning Research*, 25(38):1–46.

- Barber, R. F., Sidky, E. Y., Schmidt, T. G., and Pan, X. (2016). An algorithm for constrained one-step inversion of spectral ct data. *Physics in Medicine & Biology*, 61(10):3784.
- Beck, A. (2017). *First-Order Methods in Optimization*. Society for Industrial and Applied Mathematics.
- Beister, M., Kolditz, D., and Kalender, W. A. (2012). Iterative reconstruction methods in x-ray ct. *Physica Medica*, 28(2):94–108.
- Buzug, T. M. (2011). Computed tomography. In *Springer handbook of medical technology*, pages 311–342. Springer.
- Center for Nondestructive Evaluation, Iowa State University (2024). Computed tomography. <https://www.nde-ed.org/NDETechniques/Radiography/AdvancedTechniques/computedtomography.xhtml>. [Online; accessed on 17-July-2024].
- Chandrasekher, K. A., Pananjady, A., and Thrampoulidis, C. (2023). Sharp global convergence guarantees for iterative nonconvex optimization with random data. *The Annals of Statistics*, 51(1):179–210.
- Charisopoulos, V., Chen, Y., Davis, D., Díaz, M., Ding, L., and Drusvyatskiy, D. (2021). Low-Rank Matrix Recovery with Composite Optimization: Good Conditioning and Rapid Convergence. *Foundations of Computational Mathematics*, 21(6):1505–1593.
- Chhem, R. and Brothwell, D. (2008). Paleoradiology. *Imaging mummies and fossils*. Berlin: Springer.
- Clarke, F. and Ledyaev, Y. S. (1994). Mean value inequalities. *Proceedings of the American Mathematical Society*, 122(4):1075–1083.
- Clarke, F. H. (1975). Generalized gradients and applications. *Transactions of the American Mathematical Society*, 205:247–262.
- Clarke, F. H., Ledyaev, Y. S., Stern, R. J., and Wolenski, P. R. (2008). *Nonsmooth analysis and control theory*, volume 178. Springer Science & Business Media.
- Davis, D., Drusvyatskiy, D., and Charisopoulos, V. (2023). Stochastic algorithms with geometric step decay converge linearly on sharp functions. *Mathematical Programming*, pages 1–46.
- Davis, D., Drusvyatskiy, D., MacPhee, K. J., and Paquette, C. (2018). Subgradient methods for sharp weakly convex functions. *Journal of Optimization Theory and Applications*, 179(3):962–982.
- Dirksen, S. (2015). Tail bounds via generic chaining. *Electronic Journal of Probability*, 20.
- Douglas, J. and Rachford, H. H. (1956). On the numerical solution of heat conduction problems in two and three space variables. *Transactions of the American mathematical Society*, 82(2):421–439.
- Duchi, J., Shalev-Shwartz, S., Singer, Y., and Chandra, T. (2008). Efficient projections onto the  $l_1$ -ball for learning in high dimensions. In *Proceedings of the 25th international conference on Machine learning*, pages 272–279.
- Elbakri, I. A. and Fessler, J. A. (2003). Segmentation-free statistical image reconstruction for polyenergetic x-ray computed tomography with experimental validation. *Physics in Medicine and Biology*, 48(15):2453–2477.



- Fessler, J. and Hero, A. (1994). Space-alternating generalized expectation-maximization algorithm. *IEEE Transactions on Signal Processing*, 42(10):2664–2677.
- Frei, S., Cao, Y., and Gu, Q. (2020). Agnostic learning of a single neuron with gradient descent. *Advances in Neural Information Processing Systems*, 33:5417–5428.
- Fridovich-Keil, S., Valdivia, F., Wetzstein, G., Recht, B., and Soltanolkotabi, M. (2023). Gradient descent provably solves nonlinear tomographic reconstruction.
- Fu, L., Lee, T.-C., Kim, S. M., Alessio, A. M., Kinahan, P. E., Chang, Z., Sauer, K., Kalra, M. K., and De Man, B. (2017). Comparison Between Pre-Log and Post-Log Statistical Models in Ultra-Low-Dose CT Reconstruction. *IEEE Transactions on Medical Imaging*, 36(3):707–720.
- Geyer, L. L., Schoepf, U. J., Meinel, F. G., Nance Jr, J. W., Bastarrika, G., Leipsic, J. A., Paul, N. S., Rengo, M., Laghi, A., and De Cecco, C. N. (2015). State of the art: iterative ct reconstruction techniques. *Radiology*, 276(2):339–357.
- Gjestebj, L., De Man, B., Jin, Y., Paganetti, H., Verburg, J., Giantsoudi, D., and Wang, G. (2016). Metal artifact reduction in ct: Where are we after four decades? *IEEE Access*, 4:5826–5849.
- Goffin, J.-L. (1977). On convergence rates of subgradient optimization methods. *Mathematical programming*, 13:329–347.
- Gordon, R. (1974). A tutorial on art (algebraic reconstruction techniques). *IEEE Transactions on Nuclear Science*, 21(3):78–93.
- Hazan, E. and Kakade, S. (2019). Revisiting the Polyak step size. arXiv:1905.00313.
- Kaczmarz, S. (1993). Approximate solution of systems of linear equations. *International Journal of Control*, 57(6):1269–1271.
- Li, X., Zhu, Z., Man-Cho So, A., and Vidal, R. (2020). Nonconvex robust low-rank matrix recovery. *SIAM Journal on Optimization*, 30(1):660–686.
- Ma, C., Wang, K., Chi, Y., and Chen, Y. (2020). Implicit regularization in nonconvex statistical estimation: Gradient descent converges linearly for phase retrieval, matrix completion, and blind deconvolution. *Foundations of Computational Mathematics*, 20(3):451–632.
- Mei, S., Bai, Y., and Montanari, A. (2018). The landscape of empirical risk for nonconvex losses. *The Annals of Statistics*, 46(6A):2747–2774.
- Natterer, F. (2001). *The Mathematics of Computerized Tomography*. Society for Industrial and Applied Mathematics.
- Orlicz, W. (1932). Über eine gewisse klasse von räumen vom typus b. *Bull. Int. Acad. Pol. Ser. A*, 8(9):207–220.
- Pan, X., Sidky, E. Y., and Vannier, M. (2009). Why do commercial ct scanners still employ traditional, filtered back-projection for image reconstruction? *Inverse Problems*, 25(12):123009.
- Parikh, N. and Boyd, S. (2014). Block splitting for distributed optimization. *Mathematical Programming Computation*, 6(1):77–102.
- Polyak, B. T. (1969). Minimization of unsmooth functionals. *USSR Computational Mathematics and Mathematical Physics*, 9(3):14–29.

- Radon, J. (1917). On the determination of functions from their integrals along certain manifolds. *Mathematisch-Physische Klasse*, 69:262–277.
- Rudin, L. I., Osher, S., and Fatemi, E. (1992). Nonlinear total variation based noise removal algorithms. *Physica D: Nonlinear Phenomena*, 60(1):259–268.
- Ruszczynski, A. P. (2006). *Nonlinear optimization*. Princeton University Press.
- Sidky, E. Y. and Pan, X. (2008). Image reconstruction in circular cone-beam computed tomography by constrained, total-variation minimization. *Physics in Medicine and Biology*, 53(17):4777–4807.
- Soltanolkotabi, M. (2017). Learning relus via gradient descent. *Advances in neural information processing systems*, 30.
- Soltanolkotabi, M. (2019). Structured signal recovery from quadratic measurements: Breaking sample complexity barriers via nonconvex optimization. *IEEE Transactions on Information Theory*, 65(4):2374–2400.
- Talagrand, M. (2014). *Upper and lower bounds for stochastic processes: modern methods and classical problems*, volume 60 of *A Series of Modern Surveys in Mathematics*. Springer Science & Business Media.
- TSA (2024). Computed tomography – Transportation Security Administration. <https://www.tsa.gov/computed-tomography>. [Online; accessed on 17-July-2024].
- Vershynin, R. (2018). *High-dimensional probability: An introduction with applications in data science*, volume 47. Cambridge university press.
- Willemink, M. J., de Jong, P. A., Leiner, T., de Heer, L. M., Nijvelstein, R. A. J., Budde, R. P. J., and Schilham, A. M. R. (2013). Iterative reconstruction techniques for computed tomography - Part 1: Technical principles. *European Radiology*, 23(6):1623–1631.

## A Omitted proofs

### A.1 Proofs from Section 2

#### A.1.1 Proof of Lemma 2.1

*Proof.* Note that when  $x = \mathbf{0}$ ,  $y_i - h_i(0) = 1 - \exp(-\langle a_i, x_\star \rangle_+)$ . As a result,

$$\begin{aligned} f(0) &= \frac{1}{m} \sum_{i=1}^m 1 - \exp(-\langle a_i, x_\star \rangle_+) \\ &= 1 - \frac{1}{m} \sum_{i=1}^m \exp\left(-\|x_\star\| \left\langle a_i, \frac{x_\star}{\|x_\star\|} \right\rangle_+\right) \\ &\stackrel{(d)}{=} 1 - \frac{1}{m} \sum_{i=1}^m \exp(-(\beta_i)_+ \|x_\star\|), \quad \beta_i \sim \mathcal{N}(0, 1). \end{aligned} \quad (39)$$

We now argue the sum in (39) concentrates. To that end, we first calculate its expectation:

$$\begin{aligned} \mathbb{E}[f(0)] &= 1 - \mathbb{E}[e^{-\beta_+ \|x_\star\|}] \\ &= 1 - \frac{1}{2} \left( 1 + \exp\left(\frac{\|x_\star\|^2}{2}\right) \operatorname{erfc}\left(\frac{\|x_\star\|}{\sqrt{2}}\right) \right) \\ &= \frac{1}{2} \left( 1 - \exp\left(\frac{\|x_\star\|^2}{2}\right) \operatorname{erfc}\left(\frac{\|x_\star\|}{\sqrt{2}}\right) \right). \end{aligned}$$

To show the sum concentrates, we use the Gaussian Lipschitz inequality. We have

$$\begin{aligned} &\frac{1}{m} \sum_{i=1}^m (1 - \exp(-\langle a_i, x_\star \rangle_+)) - \frac{1}{m} \sum_{i=1}^m (1 - \exp(-\langle \tilde{a}_i, x_\star \rangle_+)) \\ &= \frac{1}{m} \sum_{i=1}^m \exp(-\langle \tilde{a}_i, x_\star \rangle_+) - \exp(-\langle a_i, x_\star \rangle_+) \\ &\leq \frac{1}{m} \sum_{i=1}^m |\langle a_i - \tilde{a}_i, x_\star \rangle| \\ &\leq \frac{\|x_\star\|}{\sqrt{m}} \|A - \tilde{A}\|_F, \quad \text{where } A = [a_1 \ \dots \ a_m]^\top, \ \tilde{A} := [\tilde{a}_1 \ \dots \ \tilde{a}_m]^\top, \end{aligned}$$

using the fact that the function  $x \mapsto \exp(-x_+)$  is 1-Lipschitz. We deduce that  $f(0)$  is Lipschitz with modulus  $\frac{\|x_\star\|}{\sqrt{m}}$  with respect to the random vectors  $\{a_i\}_{i=1, \dots, m}$ . Invoking the Gaussian Lipschitz concentration inequality (Vershynin, 2018, Theorem 5.2.2) yields

$$\mathbb{P}(|f(0) - \mathbb{E}[f(0)]| \geq t) \leq 2 \exp\left(-\frac{mt^2}{2\|x_\star\|^2}\right) \quad (40)$$

Substituting  $t = \|x_\star\| \sqrt{\frac{d}{m}}$  into (40) finishes the proof.  $\square$

#### A.1.2 Proof of Corollary 2.1

*Proof.* From Lemma B.2, we know that  $\exp(\frac{u^2}{2}) \operatorname{erfc}(\frac{u}{\sqrt{2}})$  is monotone decreasing on  $u \in (0, \infty)$ . As a result, we can lower bound the expectation by

$$\mathbb{E}[f(0)] = \frac{1}{2} \left( 1 - \exp\left(\frac{\|x_\star\|^2}{2}\right) \operatorname{erfc}\left(\frac{\|x_\star\|}{\sqrt{2}}\right) \right)$$

$$\begin{aligned}
&\geq \frac{1}{2} \left( 1 - \sqrt{e} \cdot \operatorname{erfc} \left( \frac{1}{\sqrt{2}} \right) \right) \\
&\geq \frac{1}{2} (1 - 0.53) \\
&= 0.235,
\end{aligned}$$

after numerically evaluating  $\sqrt{e} \cdot \operatorname{erfc}(1/\sqrt{2}) \leq 0.53$ . The rest follows from Lemma 2.1.  $\square$

### A.1.3 Proof of Lemma 2.2

*Proof.* We first argue that  $v_0$  is indeed a subgradient at 0. To that end, note that

$$\begin{aligned}
\partial f(x) &= \frac{1}{m} \sum_{i=1}^m \mathbf{sign}(y_i - h_i(x)) \cdot (-\partial h_i(x)) \\
&= \frac{1}{m} \sum_{i=1}^m \mathbf{sign}(y_i - h_i(x)) (-e^{-\langle a_i, x \rangle_+}) a_i \mathbb{1} \{ \langle a_i, x \rangle \geq 0 \}.
\end{aligned}$$

Note  $y_i - h_i(0) = 1 - \exp(-\langle a_i, x_\star \rangle_+) \geq 0$ . Using  $\mathbf{sign}(0) = 0$  and  $\mathbb{1} \{x \geq 0\} = 1$  for  $x \geq 0$ , we have the following expression for  $v_0$ :

$$v_0 = \frac{1}{m} \sum_{i=1}^m -a_i \mathbb{1} \{ \langle a_i, x_\star \rangle > 0 \} \Rightarrow -\langle v_0, x_\star \rangle = \frac{1}{m} \sum_{i=1}^m \langle a_i, x_\star \rangle_+ \stackrel{(d)}{=} \frac{\|x_\star\|}{m} \sum_{i=1}^m (\beta_i)_+,$$

where  $\beta_i \stackrel{\text{i.i.d.}}{\sim} \mathcal{N}(0, 1)$ . This sum has expected value

$$\mathbb{E}[-\langle v_0, x_\star \rangle] = \|x_\star\| \mathbb{E}_{X \sim \mathcal{N}(0,1)} [X_+] = \|x_\star\| \sqrt{\frac{1}{2\pi}}. \quad (41)$$

Additionally, it is  $(\|x_\star\|/\sqrt{m})$  Lipschitz as a function of  $A = (a_1, \dots, a_m)$ , since

$$\begin{aligned}
\left| \frac{1}{m} \sum_{i=1}^m \langle a_i, x_\star \rangle_+ - \langle \tilde{a}_i, x_\star \rangle_+ \right| &\leq \frac{1}{m} \sum_{i=1}^m |\langle a_i - \tilde{a}_i, x_\star \rangle| \\
&\leq \frac{\|x_\star\|}{m} \sum_{i=1}^m \|a_i - \tilde{a}_i\| \\
&\leq \frac{\|x_\star\|}{\sqrt{m}} \|A - \tilde{A}\|_F,
\end{aligned}$$

where the first inequality follows from the fact that  $x \mapsto [x]_+$  is 1-Lipschitz, the second inequality follows from Cauchy-Schwarz and the last inequality follows from norm equivalence. Applying the Gaussian concentration inequality (Vershynin, 2018, Theorem 5.2.2), we obtain

$$\mathbb{P} \left( \left| -\langle v_0, x_\star \rangle - \|x_\star\| \frac{1}{\sqrt{2\pi}} \right| \geq t \right) \leq 2 \exp \left( -\frac{mt^2}{2\|x_\star\|^2} \right)$$

Setting  $t := \|x_\star\| \sqrt{\frac{2d}{m}}$  yields (18a). For (18b), we write

$$\begin{aligned}
\|v_0\| &= \sup_{u \in \mathbb{S}^{d-1}} \frac{1}{m} \sum_{i=1}^m \langle a_i, u \rangle \mathbb{1} \{ \langle a_i, x_\star \rangle \geq 0 \} \\
&\leq \sup_{u \in \mathbb{S}^{d-1}} \frac{1}{m} \sum_{i=1}^m |\langle a_i, u \rangle|
\end{aligned}$$

$$\leq \frac{1}{\sqrt{m}} \|A\|_{\text{op}},$$

which is bounded from above by  $1 + 2\sqrt{\frac{d}{m}}$  with probability at least  $1 - \exp(-d)$  by (Vershynin, 2018, Corollary 7.3.3). This completes the proof of (18b). Finally, for (18c), we write

$$\begin{aligned} \|x_1 - x_\star\|^2 &= \|x_\star\|^2 + \frac{\eta^2 f^2(0)}{\|v_0\|^2} - 2\eta \frac{f(0)}{\|v_0\|^2} \langle v_0, 0 - x_\star \rangle \\ &= \|x_\star\|^2 - \frac{\eta f(0)}{\|v_0\|^2} (-2 \langle v_0, x_\star \rangle - \eta f(0)) \\ &\leq \|x_\star\|^2 - \frac{\eta f(0)}{\|v_0\|^2} \left( \frac{2}{\sqrt{\pi}} \|x_\star\| - \eta \right) \\ &\leq \|x_\star\|^2 - \frac{\eta f(0)}{\|v_0\|^2 \sqrt{\pi}} \|x_\star\| \\ &\leq \|x_\star\|^2 \left( 1 - \frac{\eta}{10\sqrt{\pi} \|x_\star\|} \right), \end{aligned}$$

where the first inequality follows from (18a) and  $f(0) \leq 1$ , the second inequality follows from the assumptions  $\eta \leq \frac{1}{2}$  and  $\|x_\star\| \geq 1$ , and the last inequality follows from Corollary 2.1 and (18b). This completes the proof of (18c).  $\square$

#### A.1.4 Proof of Proposition 2.1

*Proof.* Recall that the absolute value function and  $x \mapsto \exp(-x_+)$  are 1-Lipschitz. It follows that, for any pair  $x, \bar{x} \in \mathbb{R}^d$ , we have

$$\begin{aligned} f(x) - f(\bar{x}) &= \frac{1}{m} \sum_{i=1}^m |y_i - h_i(x)| - |y_i - h_i(\bar{x})| \\ &\leq \frac{1}{m} \sum_{i=1}^m |h_i(x) - h_i(\bar{x})| \\ &= \frac{1}{m} \sum_{i=1}^m |e^{-\langle a_i, x \rangle_+} - e^{-\langle a_i, \bar{x} \rangle_+}| \\ &\leq \frac{1}{m} \sum_{i=1}^m |\langle a_i, x - \bar{x} \rangle| \\ &\leq \|x - \bar{x}\| \cdot \sup_{u \in \mathbb{S}^{d-1}} \frac{1}{m} \sum_{i=1}^m \|Au\|_1 \\ &\leq \|x - \bar{x}\| \cdot \sup_{u \in \mathbb{S}^{d-1}} \frac{1}{\sqrt{m}} \|Au\| \\ &= \|x - \bar{x}\| \cdot \frac{1}{\sqrt{m}} \|A\|_{\text{op}}. \end{aligned}$$

A completely symmetric argument yields  $f(\bar{x}) - f(x) \leq \|x - \bar{x}\| \cdot \frac{\|A\|_{\text{op}}}{\sqrt{m}}$ . From (Vershynin, 2018, Corollary 7.3.3), it follows that  $\|A\|_{\text{op}} \leq \sqrt{m} + 2\sqrt{d}$  with probability at least  $1 - \exp(-d)$ . Since the latter event does not depend on the choice of  $x, \bar{x}$ , we conclude that

$$|f(x) - f(\bar{x})| \leq \|x - \bar{x}\| \cdot \left( 1 + 2\sqrt{\frac{d}{m}} \right), \quad \text{for all } x, \bar{x} \in \mathbb{R}^d,$$

with probability at least  $1 - \exp(-d)$ .  $\square$

### A.1.5 Proof of Lemma 2.3

*Proof.* The main stepping stone to (21) is the following “decrease principle” (see (Clarke et al., 2008, Theorem 3.2.8) for a version using the so-called *proximal* subdifferential):

**Claim 1** (Decrease principle). Let  $f$  be locally Lipschitz and fix  $\rho, \mu > 0$ . Suppose that

$$z \in \mathcal{B}(x; \rho), \quad \zeta \in \partial f(z) \implies \|\zeta\| \geq \mu, \quad (42)$$

Then the following inequality holds:

$$\inf_{z \in \mathcal{B}(x; \rho)} f(z) \leq f(x) - \rho\mu. \quad (43)$$

Before proving Claim 1, we show how it implies the conclusion in (21). Indeed, suppose the conclusion were false; then, for some  $x \in \mathcal{B}(x_\star; \|x_\star\|)$ , there is  $\rho > 0$  such that

$$\min(\|x - x_\star\|, \|x\|) > \rho > \frac{f(x) - f_\star}{\mu}.$$

From Lemma B.5 and  $\|x\| \leq 2\|x_\star\|$  it follows that

$$\min(\|x - x_\star\|, \|x\|, \text{dist}(x, \mathcal{B}^c(0; 3\|x_\star\|))) = \min(\|x - x_\star\|, \|x\|) > \rho > \frac{f(x) - f_\star}{\mu}. \quad (44)$$

At the same time, since  $\min(\cdot)$  is associative, we have that

$$\min(\|x\|, \text{dist}(x, \mathcal{B}^c(0; 3\|x_\star\|))) = \text{dist}(x, (\mathcal{B}(0; 3\|x_\star\|) \setminus \{0\})^c).$$

Consequently, it follows that

$$\mathcal{B}(x; \rho) \subset \mathcal{B}(0; 3\|x_\star\|) \setminus \{0\}, \quad \|x - x_\star\| > \rho.$$

The second conclusion in the display above implies that  $x \neq x_\star$ . Therefore,

$$x \in \mathcal{B}(0; 3\|x_\star\|) \setminus \{0, x_\star\} \xRightarrow{\text{(Aiming)}} \min_{v \in \partial f(x)} \|v\| \geq \mu.$$

As a result, invoking Claim 1, we obtain

$$0 \leq \inf_{\bar{x} \in \mathcal{B}(x; \rho)} f(\bar{x}) - f_\star \leq (f(x) - f_\star) - \rho\mu \stackrel{(44)}{<} 0, \quad (45)$$

which is a contradiction with our assumption that (21) fails; therefore, (21) must hold.

*Proof of Claim 1.* It remains to prove Claim 1. Since this is essentially the same as (Clarke et al., 2008, Theorem 3.2.8), with the proximal subdifferential replaced by the Clarke subdifferential, it suffices to repeat its proof with a single modification: instead of applying the version of the mean-value inequality from (Clarke et al., 2008, Theorem 3.2.6), we invoke (Clarke and Ledyaev, 1994, Theorem 4.1), which is valid for the Clarke subdifferential.  $\square$

This completes the proof of the Lemma.  $\square$

### A.1.6 Proof of Lemma 2.4

*Proof.* Recall that  $\mathbf{sign}(x) = 1$  for  $x > 0$ ,  $-1$  for  $x < 0$ , and  $\mathbf{sign}(0) = [-1, 1]$ . In turn,

$$\begin{aligned} & \mathbf{sign}(y_i - h_i(x)) \\ &= \mathbf{sign}(e^{-\langle a_i, x \rangle_+} - e^{-\langle a_i, x_\star \rangle_+}) \\ &= \mathbf{sign}(e^{-\langle a_i, x \rangle_+} - e^{-\langle a_i, x_\star \rangle_+}) \cdot (\mathbb{1}\{\langle a_i, x - x_\star \rangle \geq 0\} + \mathbb{1}\{\langle a_i, x - x_\star \rangle < 0\}) \end{aligned} \quad (46)$$

Note that it suffices to consider  $\mathbb{1}\{\langle a_i, x - x_\star \rangle > 0\}$  in the first term of (46), since

$$\frac{1}{m} \sum_{i=1}^m \mathbf{sign}(y_i - h_i(x)) e^{-\langle a_i, x \rangle} \langle a_i, x - x_\star \rangle \mathbb{1}\{\langle a_i, x \rangle \geq 0\} \mathbb{1}\{\langle a_i, x - x_\star \rangle = 0\} = 0.$$

We now proceed on a case-by-case basis.

**Case 1:**  $\langle a_i, x - x_\star \rangle < 0$ . Since all nonzero terms have  $\langle a_i, x \rangle \geq 0$ , this means

$$0 \leq \langle a_i, x \rangle < \langle a_i, x_\star \rangle \implies \langle a_i, x_\star \rangle_+ > \langle a_i, x \rangle_+ \implies \mathbf{sign}(e^{-\langle a_i, x \rangle_+} - e^{-\langle a_i, x_\star \rangle_+}) = 1,$$

via monotonicity of the exponential. This yields the partial sum

$$\begin{aligned} & \frac{1}{m} \sum_{i=1}^m \mathbf{sign}(y_i - h_i(x)) (-e^{-\langle a_i, x \rangle}) \langle a_i, x - x_\star \rangle \mathbb{1}\{\langle a_i, x \rangle \geq 0\} \mathbb{1}\{\langle a_i, x - x_\star \rangle < 0\} \\ &= \frac{1}{m} \sum_{i=1}^m e^{-\langle a_i, x \rangle} \langle a_i, x_\star - x \rangle \mathbb{1}\{\langle a_i, x \rangle \geq 0\} \mathbb{1}\{\langle a_i, x_\star - x \rangle > 0\} \\ &= \frac{1}{m} \sum_{i=1}^m e^{-\langle a_i, x \rangle} \langle a_i, x_\star - x \rangle_+ \mathbb{1}\{\langle a_i, x \rangle \geq 0\}. \end{aligned} \quad (47)$$

**Case 2(i):**  $\langle a_i, x - x_\star \rangle > 0$  and  $\langle a_i, x \rangle > 0$ . Note that we have the following possibilities:

- If  $\langle a_i, x_\star \rangle < 0$ , then  $\langle a_i, x_\star \rangle_+ = 0$ . Therefore,  $\langle a_i, x \rangle > 0$  clearly implies

$$\langle a_i, x \rangle_+ > \langle a_i, x_\star \rangle_+, \quad \text{and thus} \quad \mathbf{sign}(e^{-\langle a_i, x \rangle_+} - e^{-\langle a_i, x_\star \rangle_+}) = -1.$$

- If  $\langle a_i, x_\star \rangle \geq 0$ , then  $\langle a_i, x_\star \rangle_+ = \langle a_i, x_\star \rangle$ ; therefore,

$$\langle a_i, x \rangle_+ = \langle a_i, x \rangle > \langle a_i, x_\star \rangle = \langle a_i, x_\star \rangle_+ \implies \mathbf{sign}(e^{-\langle a_i, x \rangle_+} - e^{-\langle a_i, x_\star \rangle_+}) = -1.$$

In either instance, we obtain the partial sum

$$\begin{aligned} & \frac{1}{m} \sum_{i=1}^m \mathbf{sign}(y_i - h_i(x)) (-e^{-\langle a_i, x \rangle}) \langle a_i, x - x_\star \rangle \mathbb{1}\{\langle a_i, x \rangle > 0\} \mathbb{1}\{\langle a_i, x - x_\star \rangle > 0\} \\ &= \frac{1}{m} \sum_{i=1}^m e^{-\langle a_i, x \rangle} \langle a_i, x - x_\star \rangle \mathbb{1}\{\langle a_i, x \rangle > 0\} \mathbb{1}\{\langle a_i, x - x_\star \rangle > 0\} \\ &= \frac{1}{m} \sum_{i=1}^m e^{-\langle a_i, x \rangle} \langle a_i, x - x_\star \rangle_+ \mathbb{1}\{\langle a_i, x \rangle > 0\}. \end{aligned} \quad (48)$$



**Case 2(ii):**  $\langle a_i, x - x_\star \rangle > 0$  and  $\langle a_i, x \rangle = 0$ . In this case, we have

$$0 = \langle a_i, x \rangle > \langle a_i, x_\star \rangle \implies \langle a_i, x \rangle_+ = \langle a_i, x_\star \rangle_+ = 0.$$

As a result,  $\mathbf{sign}(y_i - h_i(x))$  can be any value between  $[-1, 1]$ . We lower bound

$$\begin{aligned} & \frac{1}{m} \sum_{i=1}^m \mathbf{sign}(y_i - h_i(x)) (-e^{-\langle a_i, x \rangle}) \langle a_i, x - x_\star \rangle \mathbb{1}\{\langle a_i, x \rangle = 0\} \mathbb{1}\{\langle a_i, x - x_\star \rangle > 0\} \\ &= \frac{1}{m} \sum_{i=1}^m \mathbf{sign}(0) \langle a_i, x_\star \rangle \mathbb{1}\{\langle a_i, x \rangle = 0\} \mathbb{1}\{\langle a_i, x - x_\star \rangle > 0\} \\ &= \frac{1}{m} \sum_{i=1}^m \mathbf{sign}(0) \cdot \langle a_i, x_\star \rangle_- \mathbb{1}\{\langle a_i, x \rangle = 0\}, \end{aligned} \tag{49}$$

using  $\langle a_i, x_\star \rangle \mathbb{1}\{\langle a_i, x_\star \rangle < 0\} = \langle a_i, x_\star \rangle_-$  in (49).

These are all the possible cases to consider. Combining Equations (47) to (49) yields

$$\begin{aligned} \langle \partial f(x), x - x_\star \rangle &= \frac{1}{m} \sum_{i=1}^m \mathbf{sign}(y_i - h_i(x)) \cdot (-e^{-\langle a_i, x \rangle}) \cdot \langle a_i, x - x_\star \rangle \mathbb{1}\{\langle a_i, x \rangle \geq 0\} \\ &= \frac{1}{m} \sum_{i=1}^m e^{-\langle a_i, x \rangle} \langle a_i, x - x_\star \rangle \mathbb{1}\{\langle a_i, x \rangle > 0\} \mathbb{1}\{\langle a_i, x - x_\star \rangle > 0\} \\ &\quad - \frac{1}{m} \sum_{i=1}^m e^{-\langle a_i, x \rangle} \langle a_i, x - x_\star \rangle \mathbb{1}\{\langle a_i, x \rangle \geq 0\} \mathbb{1}\{\langle a_i, x - x_\star \rangle < 0\} \\ &\quad + \frac{1}{m} \sum_{i=1}^m \mathbf{sign}(0) \langle a_i, x_\star \rangle_- \mathbb{1}\{\langle a_i, x \rangle = 0\} \\ &= \frac{1}{m} \sum_{i=1}^m e^{-\langle a_i, x \rangle} \langle a_i, x - x_\star \rangle \mathbb{1}\{\langle a_i, x \rangle > 0\} \mathbb{1}\{\langle a_i, x - x_\star \rangle \geq 0\} \\ &\quad + \frac{1}{m} \sum_{i=1}^m e^{-\langle a_i, x \rangle} \langle a_i, x_\star - x \rangle \mathbb{1}\{\langle a_i, x \rangle \geq 0\} \mathbb{1}\{\langle a_i, x_\star - x \rangle > 0\} \\ &\quad + \frac{1}{m} \sum_{i=1}^m \mathbf{sign}(0) \langle a_i, x_\star \rangle_- \mathbb{1}\{\langle a_i, x \rangle = 0\} \\ &= \frac{1}{m} \sum_{i=1}^m e^{-\langle a_i, x \rangle} \langle a_i, x - x_\star \rangle_+ \mathbb{1}\{\langle a_i, x \rangle > 0\} \\ &\quad + \frac{1}{m} \sum_{i=1}^m e^{-\langle a_i, x \rangle} \langle a_i, x_\star - x \rangle_+ \mathbb{1}\{\langle a_i, x \rangle \geq 0\} \\ &\quad + \frac{1}{m} \sum_{i=1}^m \mathbf{sign}(0) \langle a_i, x_\star \rangle_- \mathbb{1}\{\langle a_i, x \rangle = 0\} \\ &= \frac{1}{m} \sum_{i=1}^m e^{-\langle a_i, x \rangle} \mathbb{1}\{\langle a_i, x \rangle > 0\} (\langle a_i, x - x_\star \rangle_+ + \langle a_i, x_\star - x \rangle_+) \\ &\quad + \frac{1}{m} \sum_{i=1}^m \mathbb{1}\{\langle a_i, x \rangle = 0\} (\langle a_i, x_\star \rangle_+ + \mathbf{sign}(0) \langle a_i, x_\star \rangle_-) \end{aligned}$$

$$\begin{aligned}
&= \frac{1}{m} \sum_{i=1}^m e^{-\langle a_i, x \rangle} \mathbb{1} \{ \langle a_i, x \rangle > 0 \} \cdot | \langle a_i, x - x_\star \rangle | \\
&\quad + \frac{1}{m} \sum_{i=1}^m \mathbb{1} \{ \langle a_i, x \rangle = 0 \} ( \langle a_i, x_\star \rangle_+ + \mathbf{sign}(0) \langle a_i, x_\star \rangle_- ),
\end{aligned}$$

where the last equality follows from the identity  $[x]_+ + [-x]_+ = |x|$ .  $\square$

### A.1.7 Proof of Lemma 2.5

*Proof.* We first argue that we can effectively ignore the second term in the expression furnished by Lemma 2.4, since it corresponds to a zero-measure event (for any  $x \neq 0$ ). To show this formally, we first note that since  $\mathbf{sign}(0) = [-1, 1]$  and  $\mathbb{1} \{ \langle a_i, x \rangle = 0 \} = [0, 1]$  the contribution of the second term is always at least

$$\frac{1}{m} \sum_{i=1}^m \mathbb{1} \{ \langle a_i, x \rangle = 0 \} ( \langle a_i, x_\star \rangle_+ + \mathbf{sign}(0) \langle a_i, x_\star \rangle_- ) \geq \frac{1}{m} \sum_{i=1}^m \mathcal{I} \{ \langle a_i, x \rangle = 0 \} \langle a_i, x_\star \rangle_-,$$

where  $\mathcal{I} \{ \mathcal{E} \} = 1$  when  $\mathcal{E}$  happens and 0 otherwise. We now write

$$\begin{aligned}
\mathcal{I} \{ \langle a_i, x \rangle = 0 \} \langle a_i, x_\star \rangle_- &= \mathcal{I} \{ \langle a_i, u \rangle = 0 \} \left( \langle \cancel{a_i, u} \rangle_0^0 \langle u, x_\star \rangle + \langle P_{u^\perp} a_i, P_{u^\perp} x_\star \rangle \right)_- \\
&\stackrel{(d)}{=} \mathcal{I} \{ \langle a_i, u \rangle = 0 \} \cdot \langle \tilde{a}_i, P_{u^\perp} x_\star \rangle_-, \quad \tilde{a}_i \sim \mathcal{N}(0, I_d) \perp a_i,
\end{aligned}$$

where we write  $u = x/\|x\|$ ,  $P_{u^\perp} = (I - uu^\top)$ , and use the fact that the variables  $\langle a_i, u \rangle$  and  $P_{u^\perp} a_i$  are uncorrelated (thus independent) Gaussians to replace  $P_{u^\perp} a_i$  with an independent copy  $P_{u^\perp} \tilde{a}_i$ . From independence, it follows that

$$\begin{aligned}
\mathbb{E} [ \langle a_i, x_\star \rangle_- \mathbb{1} \{ \langle a_i, x \rangle = 0 \} ] &\geq \mathbb{E} [ \mathcal{I} \{ \langle a_i, x \rangle = 0 \} \cdot \langle a_i, x_\star \rangle_- ] \\
&= \mathbb{E} [ \mathcal{I} \{ \langle a_i, u \rangle = 0 \} ] \mathbb{E} [ \langle \tilde{a}_i, P_{u^\perp} x_\star \rangle_- ] \\
&= \mathbb{P} ( \langle \cancel{a_i, u} \rangle = 0 ) \cdot \mathbb{E} [ \langle \tilde{a}_i, P_{u^\perp} x_\star \rangle_- ] \\
&= 0,
\end{aligned} \tag{50}$$

where  $\mathbb{P} ( \langle a_i, u \rangle = 0 )$  since  $a_i$  is standard Gaussian and  $u \neq 0$ . In light of (50), we may ignore the second term in Lemma 2.4 in lower-bounding the expectation, since that term has a nonnegative contribution. Continuing from the expression furnished by Lemma 2.4, we obtain

$$\begin{aligned}
\langle \partial f(x), x - x_\star \rangle &= \frac{1}{m} \sum_{i=1}^m \exp(-\langle a_i, x \rangle) | \langle a_i, x_\star - x \rangle | \mathbb{1} \{ \langle a_i, x \rangle \geq 0 \} \\
&= \frac{\|x - x_\star\|}{m} \sum_{i=1}^m \exp(-\langle a_i, u \rangle \|x\|) | \langle a_i, v \rangle | \mathbb{1} \{ \langle a_i, u \rangle \geq 0 \} \\
&\geq \frac{\|x - x_\star\|}{m} \sum_{i=1}^m \exp(-3 \langle a_i, u \rangle \|x_\star\|) | \langle a_i, v \rangle | \mathbb{1} \{ \langle a_i, u \rangle \geq 0 \} \\
&\stackrel{(d)}{=} \frac{\|x - x_\star\|}{m} \sum_{i=1}^m \exp(-3 \beta_i \|x_\star\|) | \beta_i \langle u, v \rangle + \beta_i^\perp \|P_{u^\perp} v\| | \mathbb{1} \{ \beta_i \geq 0 \},
\end{aligned}$$

writing  $u := \frac{x}{\|x\|}$  and  $v := \frac{x_\star - x}{\|x_\star - x\|}$ . Here,  $\beta_i, \beta_i^\perp \stackrel{\text{i.i.d.}}{\sim} \mathcal{N}(0, 1)$  arise from the decomposition

$$\begin{aligned}
\langle a_i, v \rangle &= \langle uu^\top a_i, v \rangle + \langle (I - uu^\top) a_i, v \rangle \\
&= \langle a_i, u \rangle \langle u, v \rangle + \langle (I - uu^\top) a_i, v \rangle
\end{aligned}$$

$$\begin{aligned}
&\stackrel{(d)}{=} \langle a_i, u \rangle \langle u, v \rangle + \langle (I - uu^\top) \tilde{a}_i, v \rangle \quad (a_i \perp \tilde{a}_i \sim \mathcal{N}(0, I_d)) \\
&= \langle a_i, u \rangle \langle u, v \rangle + \langle \tilde{a}_i, (I - uu^\top) v \rangle \\
&\stackrel{(d)}{=} \beta_i \langle u, v \rangle + \beta_i^\perp \|(I - uu^\top) v\|,
\end{aligned}$$

writing  $\beta_i = \langle a_i, u \rangle \sim \mathcal{N}(0, 1)$  and using the identity  $\langle \tilde{a}_i, z \rangle \sim \mathcal{N}(0, \|z\|^2)$ ; we also recognize  $(I - uu^\top) = P_{u^\perp}$ . We now consider two cases for the correlation  $\langle u, v \rangle$ :

**Case 1:**  $\langle u, v \rangle \geq 0$ . In this case, we may lower bound the sum by the following expression:

$$\begin{aligned}
&\langle \partial f(x), x - x_\star \rangle \\
&\geq \frac{\|x - x_\star\|}{m} \sum_{i=1}^m \exp(-3\beta_i \|x_\star\|) |\beta_i \langle u, v \rangle + \beta_i^\perp \|P_{u^\perp} v\| \mathbb{1} \{\beta_i \geq 0, \beta_i^\perp \geq 0\} \\
&= \frac{\|x - x_\star\|}{m} \sum_{i=1}^m \exp(-3\beta_i \|x_\star\|) (\beta_i |\langle u, v \rangle| + \beta_i^\perp \|P_{u^\perp} v\|) \mathbb{1} \{\beta_i \geq 0, \beta_i^\perp \geq 0\}. \quad (51)
\end{aligned}$$

**Case 2:**  $\langle u, v \rangle < 0$ . In this case, we may lower bound the sum by the following expression:

$$\begin{aligned}
&\langle \partial f(x), x - x_\star \rangle \\
&\geq \frac{\|x - x_\star\|}{m} \sum_{i=1}^m \exp(-3\beta_i \|x_\star\|) |\beta_i \langle u, v \rangle + \beta_i^\perp \|P_{u^\perp} v\| \mathbb{1} \{\beta_i \geq 0, \beta_i^\perp \leq 0\} \\
&= \frac{\|x - x_\star\|}{m} \sum_{i=1}^m \exp(-3\beta_i \|x_\star\|) (\beta_i (-\langle u, v \rangle) - \beta_i^\perp \|P_{u^\perp} v\|) \mathbb{1} \{\beta_i \geq 0, \beta_i^\perp \leq 0\} \\
&\stackrel{(d)}{=} \frac{\|x - x_\star\|}{m} \sum_{i=1}^m \exp(-3\beta_i \|x_\star\|) (\beta_i |\langle u, v \rangle| + \tilde{\beta}_i^\perp \|P_{u^\perp} v\|) \mathbb{1} \{\beta_i, \tilde{\beta}_i^\perp \geq 0\}, \quad (52)
\end{aligned}$$

where  $\tilde{\beta}_i \sim \mathcal{N}(0, 1) \perp \beta_i$ , using the fact that the expression inside the absolute value is nonpositive. Since the sum in (52) is distributionally identical to (51), it suffices to study

$$(\natural) := \frac{1}{m} \sum_{i=1}^m \exp(-3\beta_i \|x_\star\|) (\beta_i |\langle u, v \rangle| + \beta_i^\perp \|P_{u^\perp} v\|) \mathbb{1} \{\beta_i, \beta_i^\perp \geq 0\}. \quad (53)$$

Taking expectations with respect to  $\beta$  and  $\beta^\perp$  and writing  $\gamma := 3\|x_\star\|$  for brevity, we obtain

$$\begin{aligned}
&\mathbb{E}_{\beta, \beta^\perp} [\exp(-\gamma\beta) (\beta |\langle u, v \rangle| + \beta^\perp \|P_{u^\perp} v\|) \mathbb{1} \{\beta, \beta^\perp \geq 0\}] \\
&= |\langle u, v \rangle| \cdot \mathbb{E}_\beta [\exp(-\gamma\beta) \beta_+] \cdot \mathbb{P}(\beta^\perp \geq 0) + \|P_{u^\perp} v\| \mathbb{E}_{\beta^\perp} [\beta_+] \cdot \mathbb{E}_\beta [\exp(-\gamma\beta) \mathbb{1} \{\beta \geq 0\}] \\
&= \frac{|\langle u, v \rangle|}{4} \left( \sqrt{\frac{2}{\pi}} - \gamma \exp\left(\frac{\gamma^2}{2}\right) \operatorname{erfc}\left(\frac{\gamma}{\sqrt{2}}\right) \right) + \frac{\|P_{u^\perp} v\|}{4} \sqrt{\frac{2}{\pi}} \exp\left(\frac{\gamma^2}{2}\right) \operatorname{erfc}\left(\frac{\gamma}{\sqrt{2}}\right) \\
&\geq \frac{|\langle u, v \rangle|}{4(1 + \pi\gamma^2)} \cdot \sqrt{\frac{2}{\pi}} + \frac{\|P_{u^\perp} v\|}{4} \sqrt{\frac{2}{\pi}} \exp\left(\frac{\gamma^2}{2}\right) \operatorname{erfc}\left(\frac{\gamma}{\sqrt{2}}\right) \\
&= \frac{|\langle u, v \rangle|}{4(1 + \pi\gamma^2)} \cdot \sqrt{\frac{2}{\pi}} + \frac{\|P_{u^\perp} v\|}{4\gamma} \sqrt{\frac{2}{\pi}} \cdot \gamma \exp\left(\frac{\gamma^2}{2}\right) \operatorname{erfc}\left(\frac{\gamma}{\sqrt{2}}\right) \\
&\geq \sqrt{\frac{1}{8\pi}} \cdot \min \left\{ \frac{1}{1 + \pi\gamma^2}, \frac{1}{2\gamma} \right\} (|\langle u, v \rangle| + \|P_{u^\perp} v\|) \\
&\geq \sqrt{\frac{1}{8\pi}} \cdot \frac{1}{1 + \pi\gamma^2} \|P_u v + P_{u^\perp} v\|
\end{aligned}$$

$$= \sqrt{\frac{1}{8\pi}} \frac{1}{1 + \pi\gamma^2},$$

using Lemma B.1 in the second equality, Lemma B.4 in the first inequality, Lemma B.3 and the bound  $\gamma \geq 1$  in the second inequality, the fact that  $|\langle u, v \rangle| = \|P_u v\|$  and the triangle inequality in the last inequality, and  $v \in \mathbb{S}^{d-1}$  in the last step. As a result, we have

$$\mathbb{E}[\langle \partial f(x), x - x_\star \rangle] \geq \frac{\|x - x_\star\|}{\sqrt{8\pi} (1 + 9\pi \|x_\star\|^2)}, \quad \text{for any } x \in \mathcal{B}(\mathbf{0}; 3 \|x_\star\|).$$

This is precisely the claimed lower bound, and thus completes the proof.  $\square$

### A.1.8 Proof of Proposition 2.2

*Proof.* Our proof relies on the generic chaining technique due to Talagrand (Talagrand, 2014), using the refinements of (Dirksen, 2015). Setting the stage, consider a random process indexed by a set  $\mathcal{T}$ ,  $(Z_t)_{t \in \mathcal{T}}$ . We say that  $(Z_t)$  has *mixed tails* with respect to metrics  $(d_1, d_2)$  if

$$\mathbb{P}(|Z_t - Z_s| \geq u d_1(s, t) + \sqrt{u} d_2(s, t)) \leq e^{-u}. \quad (54)$$

Under this condition, (Dirksen, 2015, Theorem 3.5) furnishes the following uniform bound: for any  $t_0 \in \mathcal{T}$ , it holds that

$$\mathbb{P}\left(\sup_{t \in \mathcal{T}} |Z_t - Z_{t_0}| \geq C(\gamma_1(\mathcal{T}, d_1) + \gamma_2(\mathcal{T}, d_2)) + u \mathbf{diam}_{d_1}(\mathcal{T}) + \sqrt{u} \mathbf{diam}_{d_2}(\mathcal{T})\right) \leq e^{-u}, \quad (55)$$

where  $\mathbf{diam}_d(\mathcal{T}) := \sup_{s, t \in \mathcal{T}} d(s, t)$  and  $\gamma_\alpha(\mathcal{T}, d)$  is the Talagrand's  $\gamma$ -functional:

$$\gamma_\alpha(\mathcal{T}, d) = \inf_{(\mathcal{T}_k)} \sup_{t \in \mathcal{T}} \sum_{k=0}^{\infty} 2^{k/\alpha} d(t, \mathcal{T}_k), \quad \mathcal{T}_k \in \left\{ \mathcal{H} \subset \mathcal{T} \mid |\mathcal{H}| \leq 2^{2^k} \right\}.$$

The first step in our proof is to verify condition (54) for the random process at hand.

**Claim 2** (Mixed tail condition). For any  $(u, v) \in \mathbb{S}^{d-1} \times \mathbb{S}^{d-1}$  and  $i \in [m]$ , define the process

$$Z_i(u, v) := \exp(-3 \langle a_i, u \rangle \|x_\star\|) |\langle a_i, v \rangle| \mathbb{1}\{\langle a_i, u \rangle > 0\} + \mathcal{I}\{\langle a_i, u \rangle = 0\} \langle a_i, x_\star \rangle_-. \quad (56)$$

Then the process  $Z(u, v) := \frac{1}{m} \sum_{i=1}^m Z_i(u, v) - \mathbb{E}[Z_i(u, v)]$  satisfies (54) with

$$d_1 = \frac{(1 + 3 \|x_\star\|) d_{\text{euc}}}{m}, \quad d_2 = \frac{(1 + 3 \|x_\star\|) d_{\text{euc}}}{\sqrt{m}},$$

where  $d_{\text{euc}}$  denotes the Euclidean metric on  $\mathbb{R}^d \times \mathbb{R}^d$ .

*Proof of Claim 2.* Let  $(u, v)$  and  $(\bar{u}, \bar{v}) \in \mathbb{S}^{d-1} \times \mathbb{S}^{d-1}$  and consider the difference  $Z_i(u, v) - Z_i(\bar{u}, \bar{v})$ . Writing  $\gamma := 3 \|x_\star\|$ , we obtain

$$\begin{aligned} \|Z_i(u, v) - Z_i(\bar{u}, \bar{v})\|_{\psi_1} &\leq \|(|\langle a_i, v \rangle| - |\langle a_i, \bar{v} \rangle|) e^{-\langle a_i, u \rangle \gamma} \mathbb{1}\{\langle a_i, u \rangle \geq 0\}\|_{\psi_1} \\ &\quad + \|(e^{-\langle a_i, u \rangle \gamma} \mathbb{1}\{\langle a_i, u \rangle \geq 0\} - e^{-\langle a_i, \bar{u} \rangle \gamma} \mathbb{1}\{\langle a_i, \bar{u} \rangle \geq 0\}) |\langle a_i, \bar{v} \rangle|\|_{\psi_1} \\ &\quad + \|\langle a_i, x_\star \rangle_- (\mathcal{I}\{\langle a_i, u \rangle = 0\} - \mathcal{I}\{\langle a_i, \bar{u} \rangle = 0\})\|_{\psi_1} \\ &\leq \| |\langle a_i, v - \bar{v} \rangle| \|_{\psi_1} + \gamma \| |\langle a_i, u - \bar{u} \rangle| |\langle a_i, \bar{v} \rangle| \|_{\psi_1} \\ &\leq \|v - \bar{v}\| + \|u - \bar{u}\| \cdot \gamma \\ &\lesssim (1 + \gamma) \left\| \begin{bmatrix} u \\ v \end{bmatrix} - \begin{bmatrix} \bar{u} \\ \bar{v} \end{bmatrix} \right\|, \end{aligned}$$

using the fact that the mapping  $x \mapsto e^{-\gamma x} \mathbb{1}\{x \geq 0\}$  is  $\gamma$ -Lipschitz on  $x \geq 0$ , as well as the property  $\|XY\|_{\psi_1} \leq \|X\|_{\psi_2} \|Y\|_{\psi_2}$  (Vershynin, 2018, Lemma 2.7.7); in particular, using the latter property implies that the last term in the decomposition satisfies

$$\begin{aligned} \|\langle a_i, x_\star \rangle_- (\mathcal{I}\{\langle a_i, u \rangle = 0\} - \mathcal{I}\{\langle a_i, \bar{u} \rangle = 0\})\|_{\psi_1} &\lesssim \|\mathcal{I}\{\langle a_i, u \rangle = 0\}\|_{\psi_2} + \|\mathcal{I}\{\langle a_i, \bar{u} \rangle = 0\}\|_{\psi_2} \\ &= 0, \end{aligned}$$

where the last line follows from (Vershynin, 2018, Proposition 2.5.2) and the identity

$$\begin{aligned} \|\mathcal{I}\{\langle a_i, u \rangle = 0\}\|_{L^p} &= (\mathbb{E}[(\mathcal{I}\{\langle a_i, u \rangle = 0\})^p])^{\frac{1}{p}} \\ &= (\mathbb{E}[\mathcal{I}\{\langle a_i, u \rangle = 0\}])^{\frac{1}{p}} \\ &= 0. \end{aligned}$$

From the Bernstein inequality (Vershynin, 2018, Corollary 2.8.3), it follows that

$$\mathbb{P}(|Z(u, v) - Z(\bar{u}, \bar{v})| \geq t) \leq 2e^{-c \min\left\{\frac{mt^2}{(1+\gamma)^2 d_{\text{euc}}^2((u, v), (\bar{u}, \bar{v}))}, \frac{mt}{(1+\gamma) d_{\text{euc}}((u, v), (\bar{u}, \bar{v}))}\right\}}, \quad (57)$$

$$\text{where } Z(u, v) := \frac{1}{m} \sum_{i=1}^m Z_i(u, v) - \mathbb{E}[Z_i(u, v)].$$

To argue that  $Z(u, v)$  has mixed tails, we let

$$d_1 = \frac{(1+\gamma)d_{\text{euc}}}{m}, \quad d_2 = \frac{(1+\gamma)d_{\text{euc}}}{\sqrt{m}}, \quad s = t \cdot d_1((u, v), (\bar{u}, \bar{v})) + \sqrt{t} \cdot d_2((u, v), (\bar{u}, \bar{v})).$$

Substituting in (57), and noting  $s \geq td_1((u, v), (\bar{u}, \bar{v}))$  and  $s^2 \geq td_2^2((u, v), (\bar{u}, \bar{v}))$ , we obtain

$$\mathbb{P}(|Z(u, v) - Z(\bar{u}, \bar{v})| \geq s) \leq 2 \exp\left(-c \min\left\{\frac{s^2}{d_2^2}, \frac{s}{d_1}\right\}\right) \leq 2e^{-ct}.$$

Relabeling and adjusting constants yields the mixed tail condition.  $\square$

With Claim 2 at hand, we can invoke (55) for  $\mathcal{T} := (\mathbb{S}^{d-1} \times \mathbb{S}^{d-1}) \cup \{\mathbf{0}\}$ :

$$\mathbb{P}\left(\sup_{u, v} |Z(u, v)| \geq C(\gamma_1(\mathcal{T}, d_1) + \gamma_2(\mathcal{T}, d_2)) + t \mathbf{diam}_{d_1}(\mathcal{T}) + \sqrt{t} \mathbf{diam}_{d_2}(\mathcal{T})\right) \leq 2e^{-t}. \quad (58)$$

To simplify (58), we bound the  $\gamma$ -functionals using Dudley's entropy integral method.

**Claim 3** (Dudley bounds I). Let  $\mathcal{T} := (\mathbb{S}^{d-1} \times \mathbb{S}^{d-1}) \cup \{\mathbf{0}\}$ . We have

$$\mathbf{diam}_{d_1}(\mathcal{T}) \lesssim \frac{(1+3\|x_\star\|)}{m}, \quad \gamma_1(\mathcal{T}, d_1) \lesssim \frac{(1+3\|x_\star\|)d}{m}. \quad (59)$$

*Proof of Claim 3.* Using Dudley's entropy integral method yields

$$\begin{aligned} \gamma_1(\mathcal{T}, d_1) &= \frac{1+\gamma}{m} \gamma_1(\mathcal{T}, \|\cdot\|) \\ &\lesssim \frac{1+\gamma}{m} \int_0^\infty \log_+ \mathcal{N}(\mathcal{T}, u) du \\ &= \frac{1+\gamma}{m} \int_0^\infty \log_+ \mathcal{N}(\mathcal{T}, u) du \\ &= \frac{1+\gamma}{m} \int_0^1 \log \mathcal{N}(\mathcal{T}, u) du \end{aligned}$$

$$\begin{aligned}
&\lesssim \frac{(1+\gamma)d}{m} \int_0^1 \log \frac{1}{\varepsilon} d\varepsilon \\
&= \frac{(1+3\|x_\star\|)d}{m},
\end{aligned}$$

using the fact that the  $\epsilon$ -covering number of the unit sphere is  $(1/\epsilon)^d$ , thus the covering number of their Cartesian product is  $(1/\epsilon)^{2d}$ . At the same time,

$$\begin{aligned}
\mathbf{diam}_{d_1}(\mathcal{T}) &= \sup_{s,t \in \mathcal{T}} d_1(s,t) \\
&= \frac{1+3\|x_\star\|}{m} \sup_{s,t \in \mathcal{T}} d_{\text{euc}}(s,t) \\
&\leq \frac{1+3\|x_\star\|}{m} \cdot \sqrt{\sup_{u,\bar{u} \in \mathbb{S}^{d-1}} \|u - \bar{u}\|^2 + \sup_{v,\bar{v} \in \mathbb{S}^{d-1}} \|v - \bar{v}\|^2} \\
&\leq \frac{2\sqrt{2}(1+3\|x_\star\|)}{m},
\end{aligned}$$

as expected. This completes the proof.  $\square$

**Claim 4** (Dudley bounds II). Let  $\mathcal{T} := (\mathbb{S}^{d-1} \times \mathbb{S}^{d-1}) \cup \{\mathbf{0}\}$ . We have

$$\mathbf{diam}_{d_2}(\mathcal{T}) \lesssim \frac{(1+3\|x_\star\|)}{\sqrt{m}}, \quad \gamma_2(\mathcal{T}, d_2) \lesssim (1+3\|x_\star\|) \sqrt{\frac{d}{m}}. \quad (60)$$

*Proof of Claim 4.* Proceeding as in the proof of Claim 3, we obtain

$$\begin{aligned}
\gamma_2(\mathcal{T}, d_2) &= \frac{1+\gamma}{\sqrt{m}} \gamma_2(\mathcal{T}, \|\cdot\|) \\
&\lesssim \frac{1+\gamma}{\sqrt{m}} \int_0^\infty \sqrt{\log \mathcal{N}(\mathcal{T}, u)} du \\
&= \frac{1+\gamma}{\sqrt{m}} \int_0^{\mathbf{diam}(\mathcal{T})} \sqrt{\log \mathcal{N}(\mathcal{T}, u)} du \\
&\lesssim \frac{(1+\gamma)\sqrt{d}}{m} \int_0^1 \sqrt{\log \frac{1}{\varepsilon}} d\varepsilon \\
&= (1+3\|x_\star\|) \sqrt{\frac{d}{m}}.
\end{aligned}$$

Similarly, to control the diameter under  $d_2$  we obtain

$$\begin{aligned}
\mathbf{diam}_{d_2}(\mathcal{T}) &= \sup_{s,t \in \mathcal{T}} d_2(s,t) \\
&= \frac{1+3\|x_\star\|}{\sqrt{m}} \sup_{s,t \in \mathcal{T}} d_{\text{euc}}(s,t) \\
&\leq \frac{1+3\|x_\star\|}{\sqrt{m}} \cdot \sqrt{\sup_{u,\bar{u} \in \mathbb{S}^{d-1}} \|u - \bar{u}\|^2 + \sup_{v,\bar{v} \in \mathbb{S}^{d-1}} \|v - \bar{v}\|^2} \\
&\leq \frac{2\sqrt{2}(1+3\|x_\star\|)}{\sqrt{m}},
\end{aligned}$$

as expected. This completes the proof.  $\square$

Combining Equation (58) and Claims 3 and 4, we obtain

$$\mathbb{P} \left( \sup_{u,v} |Z(u,v)| \geq C(1+3\|x_\star\|) \left( \sqrt{\frac{d}{m}} + \frac{d}{m} \right) \right)$$

$$\begin{aligned}
&\leq \mathbb{P} \left( \sup_{u,v} |Z(u,v)| \geq C(\gamma_1(\mathcal{T}, d_1) + \gamma_2(\mathcal{T}, d_2)) + d \cdot \mathbf{diam}_{d_1}(\mathcal{T}) + \sqrt{d} \cdot \mathbf{diam}_{d_2}(\mathcal{T}) \right) \\
&\leq 2e^{-d}.
\end{aligned}$$

By definition of  $Z(u, v)$  and Lemma 2.5, it follows that

$$\frac{1}{m} \sum_{i=1}^m \exp(-3 \langle a_i, u \rangle \|x_\star\|) |\langle a_i, v \rangle| \mathbb{1}_{\{\langle a_i, u \rangle \geq 0\}} \geq \frac{1}{\sqrt{8\pi} (1 + 9\pi \|x_\star\|^2)} - C \left( \sqrt{\frac{d}{m}} + \frac{d}{m} \right),$$

uniformly over  $u, v \in \mathbb{S}^{d-1}$ , with probability  $1 - 2e^{-d}$ . Therefore, we conclude that

$$\min_{v \in \partial f(x)} \langle v, x - x_\star \rangle \geq \frac{\|x - x_\star\|}{4\sqrt{\pi} (1 + 9\pi \|x_\star\|^2)}, \quad \forall x \in \mathcal{B}(\mathbf{0}; 3\|x_\star\|) \setminus \{\mathbf{0}\},$$

with probability at least  $1 - 2e^{-d}$ , as long as  $m \gtrsim d \cdot (1 + 9\pi \|x_\star\|^2)^2 \gtrsim d \|x_\star\|^4$ .  $\square$

## A.2 Proofs from Section 3

### A.2.1 Proof of Lemma 3.1

*Proof.* We have the following chain of inequalities:

$$\begin{aligned}
\|x_{t+1} - x_\star\|^2 &\leq (1 - \bar{\rho}) \|x_t - x_\star\|^2 \\
&\leq (1 - \bar{\rho})^t \|x_1 - x_\star\|^2 \\
&\leq (1 - \bar{\rho})^t \|x_\star\|^2,
\end{aligned}$$

using the definition of  $\mathcal{A}_{\text{slow}}(j)$ , (27), and  $x_0 = \mathbf{0}$ . By the reverse triangle inequality,

$$\|x_{t+1}\| - \|x_\star\| \leq \|x_{t+1} - x_\star\| \leq (1 - \bar{\rho})^{t/2} \|x_\star\| \implies \|x_{t+1}\| \leq \|x_\star\| (1 + (1 - \bar{\rho})^{t/2}) < 2 \|x_\star\|,$$

which proves the upper bound in  $\mathcal{B}_{\text{slow}}(t+1)$ . For the lower bound, we have

$$\begin{aligned}
\|x_t\| &= \sup_{u \in \mathbb{S}^{d-1}} \langle u, x_t \rangle \\
&\geq \frac{1}{\|x_\star\|} \langle x_\star, x_t \rangle \\
&= \frac{1}{\|x_\star\|} (\langle x_\star, x_\star \rangle + \langle x_\star, x_t - x_\star \rangle) \\
&\geq \frac{1}{\|x_\star\|} (\|x_\star\|^2 - \|x_\star\| \|x_t - x_\star\|) \\
&\geq \frac{1}{\|x_\star\|} (\|x_\star\|^2 - \|x_\star\| \|x_1 - x_\star\|) \\
&\geq \frac{1}{\|x_\star\|} \|x_\star\|^2 \left( 1 - \left( 1 - \frac{1}{20\sqrt{\pi} \|x_\star\|} \right)^{1/2} \right) \\
&= \frac{1}{40\sqrt{\pi}},
\end{aligned}$$

where the second inequality follows from Cauchy-Schwarz, the third inequality follows from  $\|x_t - x_\star\| \leq \|x_1 - x_\star\|$ , which is implied by the events  $\{\mathcal{A}_{\text{slow}}(j)\}_{j \leq t}$ , the penultimate inequality follows from (27), and the last inequality follows from the identity  $\sqrt{1-x} \leq 1 - \frac{x}{2}$ .  $\square$



### A.2.2 Proof of Lemma 3.2

*Proof.* Recall that on the event  $\mathcal{B}_{\text{slow}}(t)$ , Proposition 2.2 and Lemma 2.3 imply that

$$\begin{aligned}\langle v_t, x_t - x_\star \rangle &\geq \mu \|x_t - x_\star\|, \quad v_t \in \partial f(x_t), \\ f(x_t) &\geq \mu \min\{\|x_t - x_\star\|, \|x_t\|\},\end{aligned}$$

where  $\mu := \frac{1}{4\sqrt{\pi}(1+9\pi\|x_\star\|^2)}$ . At the same time,  $\{\mathcal{A}_{\text{slow}}(j)\}_{j < t}$  and (27) yield

$$\|x_t - x_\star\|^2 \leq (1 - \bar{\rho})^{t-1} \|x_1 - x_\star\|^2 \leq \|x_\star\|^2 \left(1 - \frac{1}{20\sqrt{\pi}\|x_\star\|}\right).$$

As a result, Lemma B.5 implies the following lower bound:

$$f(x_t) \geq \mu \min(\|x_t - x_\star\|, \|x_t\|) \geq \mu \cdot \min\left\{1, \frac{1}{40\sqrt{\pi}\|x_\star\|}\right\} \|x_t - x_\star\|. \quad (61)$$

Proceeding with the convergence analysis, we obtain

$$\begin{aligned}\|x_{t+1} - x_\star\|^2 &= \left\|x_t - \eta \frac{f(x_t)}{\|v_t\|^2} v_t - x_\star\right\|^2 \\ &= \|x_t - x_\star\|^2 + \frac{\eta^2 f(x_t)^2}{\|v_t\|^2} - 2 \frac{\eta f(x_t)}{\|v_t\|^2} \langle v_t, x_t - x_\star \rangle \\ &= \|x_t - x_\star\|^2 - \frac{\eta f(x_t)}{\|v_t\|^2} (2 \langle v_t, x_t - x_\star \rangle - \eta f(x_t)) \\ &\leq \|x_t - x_\star\|^2 - \frac{\eta f(x_t)}{\|v_t\|^2} (2\mu \|x_t - x_\star\| - \mathsf{L}\eta \|x_t - x_\star\|) \\ &\leq \|x_t - x_\star\|^2 - \frac{\eta f(x_t)\mu}{\mathsf{L}^2} \|x_t - x_\star\| \\ &\leq \|x_t - x_\star\|^2 \left(1 - \eta \left(\frac{\mu}{\mathsf{L}}\right)^2 \min\left\{1, \frac{1}{40\sqrt{\pi}\|x_\star\|}\right\}\right) \\ &= \|x_t - x_\star\|^2 (1 - \bar{\rho}),\end{aligned}$$

where the first inequality follows from the aiming inequality, the penultimate inequality follows from the requirement  $\eta \leq \frac{\mu}{\mathsf{L}}$ , and the last inequality follows from (61).  $\square$

### A.2.3 Proof of Lemma 3.3

*Proof.* Iterating the inequality from the definition of  $\mathcal{A}_{\text{slow}}(j)$ , we obtain

$$\|x_{T_0} - x_\star\|^2 \leq (1 - \bar{\rho})^{T_0} \|x_\star\|^2 < \exp(-T_0 \bar{\rho}) \|x_\star\|^2 \leq \frac{1}{4} \|x_\star\|^2,$$

where the last step follows from the inequality  $T_0 \bar{\rho} \geq \log(4)$ . Consequently,

$$\begin{aligned}\|x_{T_0}\| &\geq \frac{1}{\|x_\star\|} \langle x_\star, x_{T_0} \rangle \\ &\geq \frac{1}{\|x_\star\|} (\|x_\star\|^2 - \|x_\star\| \|x_{T_0} - x_\star\|) \\ &> \frac{1}{\|x_\star\|} \|x_\star\|^2 \left(1 - \frac{1}{2}\right) \\ &= \frac{1}{2} \|x_\star\|.\end{aligned}$$

This proves the lower bound in  $\mathcal{B}_{\text{fast}}(T_0)$ ; the upper bound follows from Lemma 3.1.  $\square$

#### A.2.4 Proof of Lemma 3.4

*Proof.* Note that by iterating the definition of  $\mathcal{A}_{\text{fast}}(j)$ , we have

$$\begin{aligned}\|x_t - x_\star\|^2 &\leq (1 - \rho)^{t-T_0} \|x_{T_0} - x_\star\|^2 \\ &\leq (1 - \rho)^{t-T_0} \frac{1}{4} \|x_\star\|^2 \\ &< \frac{1}{4} \|x_\star\|^2.\end{aligned}$$

Moreover,  $\mathcal{B}_{\text{fast}}(t)$  implies  $\|x_t\| > \frac{1}{2} \|x_\star\| \geq \|x_t - x_\star\|$ . Consequently, Lemma 2.3 yields

$$f(x_t) \geq \mu \min(\|x_t - x_\star\|, \|x_t\|) = \mu \|x_t - x_\star\|. \quad (62)$$

Repeating the convergence analysis from the proof of Lemma 3.2, we obtain

$$\begin{aligned}\|x_{t+1} - x_\star\|^2 &\leq \|x_t - x_\star\|^2 - \frac{\eta f(x_t) \mu}{\mathsf{L}^2} \|x_t - x_\star\| \\ &\leq \|x_t - x_\star\|^2 \left(1 - \eta \left(\frac{\mu}{\mathsf{L}}\right)^2\right) \\ &= \|x_t - x_\star\|^2 (1 - \rho),\end{aligned}$$

where we invoke (62) in the last inequality.  $\square$

#### A.2.5 Proof of Lemma 3.5

*Proof.* The analysis mirrors that of Lemma 3.1. First, note that

$$\begin{aligned}\|x_{t+1} - x_\star\|^2 &\leq (1 - \rho) \|x_t - x_\star\|^2 \\ &\leq (1 - \rho)^{t-T_0+1} \|x_{T_0} - x_\star\|^2 \\ &< \frac{1}{4} \|x_\star\|^2,\end{aligned}$$

which implies that  $\|x_{t+1}\| > \frac{1}{2} \|x_\star\|$  by a similar argument to that used in Lemma 3.3 and  $\|x_{t+1}\| < 2 \|x_\star\|$  by repeating the argument from Lemma 3.1 and using  $\|x_{T_0} - x_\star\| < \frac{1}{2} \|x_\star\|$ .  $\square$

#### A.2.6 Proof of Proposition 3.1

*Proof.* Suppose that  $\kappa$  is a power of 2 for simplicity. For any  $i \geq i_\star := \log_2(\kappa)$ , we have

$$\eta_i := \widehat{\kappa}_i^{-1} = 2^{-i} \leq \kappa^{-1}.$$

By Theorem 3.1, any call to Algorithm 1 with step-size  $\eta_i = \widehat{\kappa}^{-1}$  running for  $T_i$  iterations, where  $T_i$  is defined in Line 4 of Algorithm 2, will “succeed”, i.e., return a point  $x_i$  satisfying

$$f(x_i) \leq \kappa_i \left(1 - \frac{1}{\kappa_i}\right)^{\frac{T_i}{2}} f(x_0) \leq \varepsilon f(x_0).$$

Moreover, it is clear that Algorithm 2 will terminate as soon as a call to Algorithm 1 succeeds. Therefore, the total number of outer loops in Algorithm 2 is  $i_\star = \log_2(\kappa)$ .

To account for the total number of subgradient evaluations, we calculate

$$\sum_{j=0}^{i_\star} T_j = \sum_{j=0}^{\log_2(\kappa)} 2\widehat{\kappa}_j^3 \log\left(\frac{\widehat{\kappa}_j}{\varepsilon}\right) + 7\widehat{\kappa}_i^{\frac{7}{2}}$$

$$\begin{aligned}
&= 2 \cdot \left[ \sum_{j=0}^{\log_2(\kappa)} 2^{3j} \log \left( \frac{2^j}{\varepsilon} \right) + 2^{\frac{7j}{2}} \right] \\
&\leq 2 \log \left( \frac{\kappa}{\varepsilon} \right) \cdot \sum_{j=0}^{\log_2(\kappa)} 8^j + 7 \sum_{j=0}^{\log_2(\kappa)} \left( 2^{\frac{7}{2}} \right)^j \\
&= 2 \log \left( \frac{\kappa}{\varepsilon} \right) \cdot \frac{1}{7} (8 \cdot \kappa^3 - 1) + 7 \cdot \frac{\left( 2^{\frac{7}{2}} \right)^{\log_2(2\kappa)} - 1}{2^{\frac{7}{2}} - 1} \\
&\leq 3\kappa^3 \log \left( \frac{\kappa}{\varepsilon} \right) + 8\kappa^{\frac{7}{2}},
\end{aligned}$$

using the summation identity for finite geometric series in the penultimate step.  $\square$

## B Technical results

**Lemma B.1.** *For  $X \sim \mathcal{N}(0, 1)$ , we have that*

$$\mathbb{E} [e^{-cX} \mathbb{1} \{X \geq 0\}] = \frac{1}{2} \exp \left( \frac{c^2}{2} \right) \operatorname{erfc} \left( \frac{c}{\sqrt{2}} \right), \quad (63a)$$

$$\mathbb{E} [e^{-cX} X_+] = \frac{1}{2} \left( \sqrt{\frac{2}{\pi}} - c \exp \left( -\frac{c^2}{2} \right) \operatorname{erfc} \left( \frac{c}{\sqrt{2}} \right) \right). \quad (63b)$$

*Proof.* The first expectation is the integral

$$\begin{aligned}
\mathbb{E} [e^{-cX} \mathbb{1} \{X \geq 0\}] &= \int_0^\infty \frac{1}{\sqrt{2\pi}} \exp \left( -\frac{x^2}{2} - cx \right) dx \\
&= \int_0^\infty \frac{1}{\sqrt{2\pi}} \exp \left( -\left( \frac{x^2}{2} + cx + \frac{c^2}{2} \right) \right) \exp \left( \frac{c^2}{2} \right) dx \\
&= \exp \left( \frac{c^2}{2} \right) \int_0^\infty \frac{1}{\sqrt{2\pi}} \exp \left( -\frac{(x+c)^2}{2} \right) dx \\
&= \exp \left( \frac{c^2}{2} \right) \int_{\frac{c}{\sqrt{2}}}^\infty \frac{1}{\sqrt{\pi}} \exp(-z^2) dz \quad (z \leftarrow \frac{x+c}{\sqrt{2}}) \\
&= \exp \left( \frac{c^2}{2} \right) \frac{1}{2} \cdot \frac{2}{\sqrt{\pi}} \int_{\frac{c}{\sqrt{2}}}^\infty \exp(-z^2) dz \\
&= \frac{1}{2} \exp \left( \frac{c^2}{2} \right) \operatorname{erfc} \left( \frac{c}{\sqrt{2}} \right),
\end{aligned}$$

using (14) in the last equality; this proves (63a). The second expectation is

$$\begin{aligned}
\mathbb{E} [e^{-cX} X_+] &= \int_0^\infty \frac{x}{\sqrt{2\pi}} \exp \left( -\frac{x^2}{2} - cx \right) dx \\
&= \int_0^\infty \frac{(x+c)}{\sqrt{2\pi}} \exp \left( -\frac{x^2}{2} - cx \right) dx - c \cdot \int_0^\infty \frac{1}{\sqrt{2\pi}} \exp \left( -\frac{x^2}{2} - cx \right) dx \\
&= \exp \left( \frac{c^2}{2} \right) \int_{\frac{c}{\sqrt{2}}}^\infty z \cdot \sqrt{\frac{2}{\pi}} \exp(-z^2) dz - \frac{c}{2} \exp \left( \frac{c^2}{2} \right) \operatorname{erfc} \left( \frac{c}{\sqrt{2}} \right),
\end{aligned}$$

recognizing the integral from (63a) in the second term. Note that

$$\frac{d}{dz} e^{-z^2} = -2ze^{-z^2} \implies \int_0^\infty z \cdot \sqrt{\frac{2}{\pi}} e^{-z^2} dz = -\sqrt{\frac{2}{\pi}} \frac{1}{2} \left\{ e^{-z^2} \right\}_{\frac{c}{\sqrt{2}}}^\infty = \frac{1}{2} \exp \left( -\frac{c^2}{2} \right) \sqrt{\frac{2}{\pi}},$$

cancelling out the leading  $\exp(c^2/2)$ ; this proves (63b).  $\square$

**Lemma B.2.** *The function  $f(x) := \exp(x^2) \cdot \operatorname{erfc}(x)$  is monotone decreasing for  $x \geq 0$ .*

*Proof.* The first derivative of  $f$  is equal to

$$f'(x) = 2x \cdot \exp(x^2) \operatorname{erfc}(x) - \frac{2}{\sqrt{\pi}}.$$

We now use the inequality  $\operatorname{erfc}(x) \leq \frac{2e^{-x^2}}{\sqrt{\pi}(x + \sqrt{x^2 + 4/\pi})}$ , which yields

$$\begin{aligned} f'(x) &\leq 2x \cdot \frac{2}{\sqrt{\pi}} \cdot \frac{1}{x + \sqrt{x^2 + 4/\pi}} - \frac{2}{\sqrt{\pi}} \\ &< \frac{4x}{\sqrt{\pi}} \cdot \frac{1}{2x} - \frac{2}{\sqrt{\pi}} \\ &\leq 0, \end{aligned}$$

which completes the proof of the claim.  $\square$

**Lemma B.3.** *The function  $\varphi(x) := x \exp(x^2) \cdot \operatorname{erfc}(x)$  is monotone increasing for  $x \geq 0$ .*

*Proof.* The first derivative of  $\varphi$  is

$$\varphi'(x) = \exp(x^2)(2x^2 + 1) \operatorname{erfc}(x) - \frac{2x}{\sqrt{\pi}}$$

Clearly,  $\varphi'(0) > 0$ . Now for any  $x > 0$ , we have

$$\begin{aligned} e^{x^2} \operatorname{erfc}(x) &\geq \frac{2}{\sqrt{\pi}(x + \sqrt{x^2 + 2})} \\ &= \frac{2}{\sqrt{\pi}} \frac{1}{x \left(1 + \sqrt{1 + \frac{2}{x^2}}\right)} \\ &\stackrel{(\sharp)}{>} \frac{2}{x\sqrt{\pi}} \frac{1}{2 + \frac{1}{x^2}} \\ &= \frac{2}{\sqrt{\pi}} \frac{1}{2x + \frac{1}{x}} \\ &= \frac{2x}{\sqrt{\pi}} \frac{1}{2x^2 + 1}, \end{aligned}$$

where  $(\sharp)$  follows from  $\sqrt{1 + x} < 1 + \frac{x}{2}$ , valid for any  $x > 0$ . Finally, multiplying with  $(2x^2 + 1)$  and subtracting  $2x/\sqrt{\pi}$  yields  $\varphi'(x) > 0$  for any  $x > 0$ , completing the proof.  $\square$

**Lemma B.4.** *For any  $x \geq 1$ , the following bound holds:*

$$x \exp\left(\frac{x^2}{2}\right) \operatorname{erfc}\left(\frac{x}{\sqrt{2}}\right) \leq \sqrt{\frac{2}{\pi}} \left(1 - \frac{1}{1 + \pi x^2}\right). \quad (64)$$

*Proof.* Starting from the known inequality

$$\operatorname{erfc}(x) \leq \frac{2e^{-x^2}}{\sqrt{\pi}(x + \sqrt{x^2 + \frac{4}{\pi}})},$$

we successively obtain

$$x \exp(x^2/2) \operatorname{erfc}(x/\sqrt{2}) \leq \frac{2x}{\sqrt{\pi}} \frac{1}{\frac{x}{\sqrt{2}} + \sqrt{\frac{x^2}{2} + \frac{4}{\pi}}}$$

$$\begin{aligned}
&= \frac{2\sqrt{2}}{\sqrt{\pi}} \frac{1}{1 + \sqrt{1 + \frac{8}{\pi x^2}}} \\
&\leq \frac{2\sqrt{2}}{\sqrt{\pi}} \frac{1}{2 + \frac{2}{\pi x^2}} \\
&= \sqrt{\frac{2}{\pi}} \frac{1}{1 + \frac{1}{\pi x^2}},
\end{aligned}$$

where the last inequality is due to the fact that

$$\sqrt{1 + y^2} \geq 1 + \frac{y^2}{4}, \quad \forall y \in [0, 1].$$

Finally, we rewrite the last fraction as

$$\frac{1}{1 + \frac{1}{\pi x^2}} = \frac{1 + \frac{1}{\pi x^2}}{1 + \frac{1}{\pi x^2}} - \frac{\frac{1}{\pi x^2}}{1 + \frac{1}{\pi x^2}} = 1 - \frac{1}{\pi x^2 + 1}.$$

This completes the proof of (64). □

**Lemma B.5.** *Suppose that  $x$  satisfies  $\|x - x_\star\|^2 < (1 - \delta) \|x_\star\|^2$ . Then*

$$\min(\|x - x_\star\|, \|x\|, \text{dist}(x, \mathcal{B}^c(\mathbf{0}; 3\|x_\star\|))) \geq \min\left\{1, \frac{\delta}{2\sqrt{1 - \delta}}\right\} \cdot \|x - x_\star\|.$$

*Proof.* We have the following sequence of inequalities:

$$\begin{aligned}
\text{dist}(x, \mathcal{B}^c(\mathbf{0}; 3\|x_\star\|)) &= \|x - \text{proj}_{\mathcal{B}^c(\mathbf{0}; 3\|x_\star\|)}(x)\| \\
&= \|x - x_\star + x_\star - \text{proj}_{\mathcal{B}^c(\mathbf{0}; 3\|x_\star\|)}(x)\| \\
&\geq \|x_\star - \text{proj}_{\mathcal{B}^c(\mathbf{0}; 3\|x_\star\|)}(x)\| - \|x - x_\star\| \\
&\geq \|x_\star - \text{proj}_{\mathcal{B}^c(\mathbf{0}; 3\|x_\star\|)}(x_\star)\| - \|x - x_\star\| \\
&> \|x_\star - \text{proj}_{\mathcal{B}^c(\mathbf{0}; 3\|x_\star\|)}(x_\star)\| - \|x_\star\| \\
&\geq 2\|x_\star\| - \|x_\star\| \\
&> \|x - x_\star\|,
\end{aligned}$$

which follow from  $\|x - \text{proj}_C(y)\| \geq \|x - \text{proj}_C(x)\|$ , our assumptions on  $\|x - x_\star\|$ , and

$$\|x_\star - \text{proj}_{\mathcal{B}^c(\mathbf{0}; 3\|x_\star\|)}(x_\star)\| \geq \|\text{proj}_{\mathcal{B}^c(\mathbf{0}; 3\|x_\star\|)}(x_\star)\| - \|x_\star\| \geq 3\|x_\star\| - \|x_\star\| = 2\|x_\star\|.$$

This shows that  $\|x - x_\star\| < \text{dist}(x, \mathcal{B}^c(\mathbf{0}; 3\|x_\star\|))$ . At the same time,

$$\begin{aligned}
(1 - \delta) \|x_\star\|^2 &\geq \|x - x_\star\|^2 \\
&= \|x\|^2 + \|x_\star\|^2 - 2\langle x, x_\star \rangle \\
&\geq \|x_\star\|^2 - 2\langle x, x_\star \rangle \\
&\Leftrightarrow \left\langle x, \frac{x_\star}{\|x_\star\|} \right\rangle \geq \frac{\delta}{2} \|x_\star\|.
\end{aligned}$$

From the previous display and our assumption  $\|x - x_\star\| \leq \sqrt{1 - \delta} \|x_\star\|$ , we deduce

$$\begin{aligned}
\|x\| &= \sup_{u \in \mathbb{S}^{d-1}} \langle x, u \rangle \\
&\geq \left\langle x, \frac{x_\star}{\|x_\star\|} \right\rangle
\end{aligned}$$

$$\begin{aligned}
&\geq \frac{\delta}{2} \|x_\star\| \\
&= \frac{\delta}{2} \frac{\|x_\star\|}{\|x - x_\star\|} \cdot \|x - x_\star\| \\
&\geq \frac{\delta}{2\sqrt{1-\delta}} \|x - x_\star\|,
\end{aligned}$$

which completes the proof of the claim.  $\square$

## C Projecting to the TV norm ball

In this section, we describe an iterative approach based on the Douglas-Rachford splitting method (Douglas and Rachford, 1956) to compute the orthogonal projection onto the TV ball. First, we rewrite

$$\begin{aligned}
\text{proj}_{\mathcal{X}}(y) &= \underset{x}{\operatorname{argmin}} \left\{ \frac{1}{2} \|x - y\|^2 \mid \|\mathbf{M}(x)\|_{\text{TV}} \leq \lambda \right\} \\
&= \underset{x}{\operatorname{argmin}} \left\{ \frac{1}{2} \|x - y\|^2 \mid \|z\|_{n^2,2} \leq \lambda, J_{\text{TV}}(x) = z \right\} \\
&= \underset{x,z}{\operatorname{argmin}} \left\{ \frac{1}{2} \|x - y\|^2 + \delta_{\{\|\cdot\|_{n^2,2} \leq \lambda\}}(z) \mid J_{\text{TV}}(x) = z \right\} \\
&= \underset{x,z}{\operatorname{argmin}} \left\{ \frac{1}{2} \|x - z\|^2 + \delta_{(\mathbb{R}^{n^2}) \times \{\|\cdot\|_{n^2,2} \leq \lambda\}}(x, z) + \delta_{\mathbf{gph}(J_{\text{TV}})}(x, z) \right\}
\end{aligned}$$

where  $\delta_{\mathcal{C}}(x) = 0$  for  $x \in \mathcal{C}$  and  $+\infty$  otherwise. The operator  $J_{\text{TV}} : \mathbb{R}^{n^2} \rightarrow \mathbb{R}^{2n^2}$  is given by

$$[J_{\text{TV}}(x)]_{(i-1) \cdot n + j} = \mathbf{M}(x)_{i+1,j} - \mathbf{M}(x)_{i,j}, \quad i, j = 1, \dots, n-1 \quad (65a)$$

$$[J_{\text{TV}}(x)]_{n^2 + (i-1) \cdot n + j} = \mathbf{M}(x)_{i,j+1} - \mathbf{M}(x)_{i,j}, \quad i, j = 1, \dots, n-1 \quad (65b)$$

and  $\|z\|_{k,2} : \mathbb{R}^{2k} \rightarrow \mathbb{R}^k$  is the following group norm:

$$\|z\|_{k,2} = \sum_{i=1}^k \|(Z_i, Z_{k+i})\|. \quad (66)$$

With this in hand, we can now write

$$\text{proj}_{\mathcal{X}}(y) = \underset{x,z}{\operatorname{argmin}} \{h_1(x, z) + h_2(x, z)\}, \quad (67a)$$

$$h_1(x, z) := \frac{1}{2} \|x - y\|^2 + \delta_{\mathbb{R}^{n^2} \times \{\|\cdot\|_{n^2,2} \leq \lambda\}}(x, z) \quad (67b)$$

$$h_2(x, z) := \delta_{\mathbf{gph}(J_{\text{TV}})}(x, z). \quad (67c)$$

The formulation in (67a) lends itself to various splitting algorithms; our implementation uses the Douglas-Rachford splitting method. The latter maintains an auxiliary sequence  $(\bar{x}, \bar{z})$ , as well as the primal iterates  $(x, z)$ , and alternates between the following steps:

$$\begin{aligned}
(x_{k+1}, z_{k+1}) &:= \mathbf{prox}_{h_1}(\bar{x}_k, \bar{z}_k); \\
(\bar{x}_{k+1}, \bar{z}_{k+1}) &:= (\bar{x}_k, \bar{z}_k) + \mathbf{prox}_{h_2}(2 \cdot (x_{k+1}, z_{k+1}) - (\bar{x}_k, \bar{z}_k)) - (x_{k+1}, z_{k+1}).
\end{aligned}$$

We now provide low-complexity formulas for the proximal operators involved when using the Douglas-Rachford splitting method to compute a projection onto the norm ball  $\|\mathbf{M}(x)\|_{\text{TV}} \leq \lambda$ . Throughout, we fix

$$h_1 : \mathbb{R}^{n^2 \times 2n^2} \rightarrow \mathbb{R}, \quad h_1(x, z) := \frac{1}{2} \|x - y\|^2 + \delta_{\mathbb{R}^{n^2} \times \{\|\cdot\|_{n^2,2} \leq \lambda\}}(x, z), \quad (68a)$$

$$h_2 : \mathbb{R}^{n^2 \times 2n^2} \rightarrow \mathbb{R}, \quad h_2(x, z) := \delta_{\mathbf{gph}(J_{\text{TV}})}(x, z), \quad (68b)$$

where  $\|z\|_{k,2} : \mathbb{R}^k \rightarrow \mathbb{R}$  is the following group norm:

$$\|z\|_{k,2} := \sum_{i=1}^k \|(z_i \quad z_{k+i})\|.$$

**Lemma C.1.** *We have the following formulas:*

$$\mathbf{prox}_{h_1}(x, z) = \left[ \text{proj}_{\|\cdot\|_{n^2,2} \leq \lambda} \left( \begin{smallmatrix} x+y \\ 2 \end{smallmatrix} \right) \right], \quad (69a)$$

$$\mathbf{prox}_{h_2}(x, z) = \text{proj}_{\mathbf{gph}(J_{\text{TV}})}(x, z). \quad (69b)$$

*Proof.* We start from the following characterization:

$$(x_+, z_+) = \mathbf{prox}_{h_1}(x, z) \Leftrightarrow (x - x_+, z - z_+) \in \partial h_1(x_+, z_+).$$

To compute  $\partial h_1$ , we use the following properties (see, e.g., (Ruszczynski, 2006)):

- $\partial \delta_{\mathcal{C}}(\bar{x}) = \mathcal{N}_{\mathcal{C}}(\bar{x})$ , where  $\mathcal{N}_{\mathcal{C}}(\bar{x})$  is the normal cone of  $\mathcal{C}$  at  $\bar{x}$ ;
- $\mathcal{N}_{\mathcal{C}_1 \times \mathcal{C}_2}(\bar{x}, \bar{z}) = \mathcal{N}_{\mathcal{C}_1}(\bar{x}) \times \mathcal{N}_{\mathcal{C}_2}(\bar{z})$  for any convex  $\mathcal{C}_1, \mathcal{C}_2$ .

Indeed, from the above it follows that

$$\begin{aligned} \partial h_1(x_+, z_+) &= (x_+ - y, \mathbf{0}) + \mathcal{N}_{\mathbb{R}^{n^2} \times \{\|\cdot\|_{n^2,2} \leq \lambda\}}(x_+, z_+) \\ &= (x_+ - y, \mathbf{0}) + \mathcal{N}_{\mathbb{R}^{n^2}}(x_+) \times \mathcal{N}_{\{\|\cdot\|_{n^2,2} \leq \lambda\}}(z_+) \\ &= (x_+ - y, \mathbf{0}) + \{\mathbf{0}_{n^2}\} \times \mathcal{N}_{\{\|\cdot\|_{n^2,2} \leq \lambda\}}(z_+) \end{aligned}$$

In particular, since this system is separable, we obtain

$$\begin{aligned} x - x_+ = (x_+ - y) &\implies x_+ = \frac{x + y}{2}, \\ z - z_+ \in \mathcal{N}_{\{\|\cdot\|_{n^2,2} \leq \lambda\}}(z_+) &\implies z_+ = \text{proj}_{\{\|\cdot\|_{n^2,2} \leq \lambda\}}(z). \end{aligned}$$

We defer the derivation of a formula for the projection to Lemma C.2. Finally, we note

$$(x_+, z_+) = \mathbf{prox}_{h_2}(x, z) \Leftrightarrow (x_+, z_+) = \text{proj}_{\mathbf{gph}(J_{\text{TV}})}(x, z).$$

Since  $J_{\text{TV}}$  is a very sparse linear operator, the graph projection can be computed very efficiently using a cached sparse Cholesky or a sparse LDLt factorization, allowing for repeated linear system solves. We defer the details to Lemma C.4.  $\square$

**Lemma C.2.** *Let  $M \in \mathbb{R}^{m \times n}$  and write  $\|M\|_{1,2} = \sum_{i=1}^m \|M_{i,:}\|$ . Then we have that*

$$\text{proj}_{\{M\|M\|_{1,2} \leq \lambda\}}(X) = \mathbf{prox}_{\mu_{\star}\|M\|_{1,2}}(X),$$

where  $\mu_{\star}$  is the unique root of the one-dimensional equation

$$\|\mathbf{prox}_{\mu\|M\|_{1,2}}(X)\|_{1,2} - \lambda = 0.$$

In particular,  $\mu_{\star}$  can be found in  $O(m \log m + mn)$  time.

*Proof.* Consider the optimality condition for the projection problem:

$$\begin{aligned} X_+ = \text{proj}_{\{U \|U\|_{1,2} \leq \lambda\}}(X) &\Leftrightarrow X - X_+ \in \mathcal{N}_{\{U \|U\|_{1,2} \leq \lambda\}}(X_+) = \mathbb{R}_+(\partial \|\cdot\|_{1,2})(X_+) \\ &\Leftrightarrow \exists \mu > 0 : (X - X_+) \in \mu(\partial \|\cdot\|_{1,2})(X_+), \quad \|X_+\|_{1,2} = \lambda \\ &\Leftrightarrow \exists \mu > 0 : \lambda = \|\mathbf{prox}_{\mu\|\cdot\|_{1,2}}(X)\|_{1,2}, \end{aligned}$$

using the property that  $\mathcal{N}_{\{X \|X\| \leq \lambda\}} = \mathbb{R}_+(\partial \|\cdot\|)$  for any norm  $\|\cdot\|$ . Examining the resulting one-dimensional equation, we note that Lemma C.3 implies that

$$\|\mathbf{prox}_{\mu\|\cdot\|_{1,2}}(X)\|_{1,2} = \lambda \Leftrightarrow \sum_{i=1}^m [\|X_{i,:}\| - \mu]_+ = \lambda. \quad (70)$$

Finally, we can use the algorithm proposed by (Duchi et al., 2008) to solve for  $\mu$  in (70). The algorithm involves a precomputation step for all row norms, achievable in time  $O(mn)$ , and a sorting step that takes time  $O(m \log m)$ . This completes the proof of the claim.  $\square$

**Lemma C.3.** *Let  $M \in \mathbb{R}^{m \times n}$  and write  $\|M\|_{1,2} = \sum_{i=1}^m \|M_{i,:}\|$ . Then for any  $\mu > 0$ ,*

$$\mathbf{prox}_{\mu\|\cdot\|_{1,2}}(X) = \begin{bmatrix} X_{1,:} \left(1 - \frac{\mu}{\max(\|X_{1,:}\|, \mu)}\right) & \cdots & X_{m,:} \left(1 - \frac{\mu}{\max(\|X_{m,:}\|, \mu)}\right) \end{bmatrix}^\top \quad (71)$$

$$\|\mathbf{prox}_{\mu\|\cdot\|_{1,2}}(X)\|_{1,2} = \sum_{i=1}^m [\|X_{i,:}\| - \mu]_+. \quad (72)$$

*Proof.* Note that  $\|M\|_{1,2}$  is separable across rows. We write

$$\begin{aligned} \mathbf{prox}_{\mu\|\cdot\|_{1,2}}(M) &= \underset{X}{\operatorname{argmin}} \left\{ \frac{1}{2\mu} \|X - M\|_F^2 + \|X\|_{1,2} \right\} \\ &= \underset{\{X_{i,:}\}_{i=1}^m}{\operatorname{argmin}} \sum_{i=1}^m \left\{ \frac{1}{2\mu} \|X_{i,:} - M_{i,:}\|^2 + \|M_{i,:}\| \right\} \\ &= \mathbf{prox}_{\mu\|\cdot\|}(M_{1,:}) \times \cdots \times \mathbf{prox}_{\mu\|\cdot\|}(M_{m,:}). \end{aligned}$$

From standard results (Beck, 2017, Example 6.19), we know that

$$\mathbf{prox}_{\mu\|\cdot\|}(M_{i,:}) = M_{i,:} \cdot \left(1 - \frac{\mu}{\max(\|M_{i,:}\|, \mu)}\right).$$

This yields the expression in (71). For (72), we first note that

$$\|X_{i,:}\| \left(1 - \frac{\mu}{\max(\|X_{i,:}\|, \mu)}\right) = \begin{cases} 0, & \|X_{i,:}\| < \mu, \\ \|X_{i,:}\| - \mu, & \text{otherwise.} \end{cases}$$

Therefore, the sum of individual norms yields precisely the right-hand side of (72).  $\square$

**Lemma C.4.** *Let  $J_{\text{TV}}$  be defined in (65a)-(65b). Then*

$$\text{proj}_{\mathbf{gph}(J_{\text{TV}})}(x, z) = \begin{bmatrix} I_{n^2} & J_{\text{TV}}^\top \\ J_{\text{TV}} & -I_{2n^2} \end{bmatrix}^{-1} \begin{bmatrix} x + J_{\text{TV}}^\top z \\ \mathbf{0}_{2n^2} \end{bmatrix}.$$

Moreover, it can be computed efficiently given a cached *LDLt* or Cholesky factorization.



*Proof.* For an arbitrary linear operator  $A$ , we have (Parikh and Boyd, 2014):

$$(x, y) = \text{proj}_{\text{gph}(A)}(\bar{x}, \bar{y}) \Leftrightarrow \begin{bmatrix} I & A^\top \\ A & -I \end{bmatrix} \begin{bmatrix} x \\ y \end{bmatrix} = \begin{bmatrix} \bar{x} + A^\top \bar{y} \\ \mathbf{0} \end{bmatrix}.$$

When  $A = J_{\text{TV}}$  and viewing  $J_{\text{TV}}$  as a linear operator from  $\mathbb{R}^{n^2} \rightarrow \mathbb{R}^{2n^2}$ , we have

$$\text{nnz} \left( \begin{bmatrix} I_{n^2} & J_{\text{TV}}^\top \\ J_{\text{TV}} & -I_{2n^2} \end{bmatrix} \right) = O(n^2),$$

which means that the matrix on the left-hand side can be factorized using an LDLt factorization. Alternatively, eliminating  $y$  from the system yields the updates

$$x = (I + J_{\text{TV}}^\top J_{\text{TV}})^{-1}(\bar{x} + J_{\text{TV}}^\top \bar{y}), \quad y = J_{\text{TV}}(x).$$

In the above, we can compute a Cholesky factorization of  $I + J_{\text{TV}}^\top J_{\text{TV}}$  and solve the resulting linear systems with low computational effort.  $\square$

## D An $f_\star$ -adaptive variant of Algorithm 1

We describe a variant of Algorithm 1 for problems with unknown optimal value  $f_\star$ , such as CT problems with noisy measurements, due to Hazan and Kakade (2019); see Algorithm 3 below.

---

**Algorithm 3** PolyakSGM-NoOpt (Hazan and Kakade, 2019, Algorithm 2)

---

- 1: **Input:**  $x_0 \in \mathbb{R}^d$ , lower bound  $\tilde{f}_0 \leq f_\star$ ,  $\eta \in (0, 1)$ , budgets  $T_{\text{inner}}, T_{\text{outer}} \in \mathbb{N}$ .
  - 2: **for**  $t = 1, \dots, T_{\text{outer}}$  **do**
  - 3:   Compute  $\hat{x}_t := \text{PolyakSGM}(x_0, \frac{\eta}{2}, T_{\text{inner}}, \tilde{f}_{t-1})$     $\triangleright$  Alg. 1 with opt. value estimate  $\tilde{f}_{t-1}$
  - 4:   Update  $\tilde{f}_t := \frac{1}{2} (f(\hat{x}_t) + \tilde{f}_{t-1})$
  - 5: **return**  $\text{argmin}_z \{f(z) \mid z \in \{\hat{x}_i\}_{i=1}^{T_{\text{outer}}}\}$ .
- 

At a high-level, Algorithm 3 maintains an estimate  $\tilde{f}_t$  of the optimal value  $f_\star$ , which is updated using the objective value found by successive calls to Algorithm 1. In particular, Hazan and Kakade (2019) show that if  $\tilde{f}_0 \leq f_\star$ , running Algorithm 3 is equivalent to running Algorithm 1 with the “correct” value of  $f_\star$ , stepsize  $\frac{\eta}{2}$ , and budget  $T_{\text{inner}}$ . Their analysis is for the case where  $f$  is convex (and thus  $\eta = 1$  is optimal); while it can be extended to our setting, under the restriction  $\eta \leq \frac{1}{\kappa}$ , we do not pursue this generalization here.